Morphological Effects of Water Soluble Polymer Flocculants Synthesized by Controlled Reversible-Deactivation Radical Polymerization for Treatment of Mature Fine Tailings

by

Benjamin Nguyen

A thesis submitted in partial fulfillment of the requirements for the degree of

Master of Science

in

Chemical Engineering

Department of Chemical and Materials Engineering

University of Alberta

Abstract

The bitumen reserves in Northern Alberta are a valuable asset, but extracting bitumen from oil sands via the Clark hot water process produces undesirable waste tailings. These tailings are transported to tailings ponds where the sand and clay particles are left to settle slowly, creating a long-term environmental problem. The most troublesome component of oil sands tailings is the mature fine tailings (MFT) component. Without additional treatment, the fine clay particles that are part of MFT may never settle completely, remaining in a mud-like suspension that endangers the environment.

One of the methods to treat these tailings is to add water-soluble polymer flocculants to create large flocs that settle to the bottom of the ponds, allowing the supernatant water to be recovered and reused in the oil extraction process.

Poly((vinylbenzyl)trimethylammonium chloride), PVB, a cationic and partially hydrophobic polymer, is the focus of this thesis. Its positive charges make it adsorb strongly on the negatively-charged clay particles, and its partial hydrophobicity produces flocs that retain less water. This thesis investigates how the configuration of PVB (linear, 3-arm, and 4-arm star) affects its MFT flocculation and dewatering performance. Atom transfer radical polymerization was used to make PVB with precisely controlled morphologies.

The 3-arm star polymer outperformed its linear counterpart at every polymer dosage in initial settling rate tests, while the 4-arm star polymer performed well only at high dosages. In general, higher dosages led to slightly greater turbidities than lower dosages, but it should be noted that suspensions obtained

at all dosages were very clear. Dewaterability was measured by comparing capillary suction times of the flocculated suspensions and the settled sediments. All polymers performed virtually the same in this test. Similarly, all polymers produced sediments with similar solids contents. The 4-arm star polymer at low dosages, however, had the worst performance in terms of settling time, relative turbidity, and capillary suction time.

Acknowledgements

It has been a privilege to have had the opportunity to complete my MSc here at the University of Alberta. I want to firstly express my deepest gratitude to Dr. João Soares for accepting me as one of his students. It has been a honour to learn from you and have your guidance in my work. From my time as one of your undergraduate research assistants to now at the end of the road of my MSc, I have and will always remember your dedication, intellect, and kindness that you have showed all of us. To all my colleagues, I thank you for the last few years in which we shared our knowledge and supported each others work. I am truly grateful to have had the chance to get to know everyone.

I want to express my deepest thanks to all my friends and family for all the love and support they've provided me. I truly appreciate my parents, siblings, and Steph for believing in me throughout this time. Finally, I have to thank my dog Zeus for being the greatest companion I could have ever asked for.

Contents

List of Tables

List of Figures

Chapter 1

General Introduction

Through the perpetual cycle of life and death coupled with the inevitable passage of time, heat and pressure transform organic matter deep underground into various fossil fuels. For decades, these fuels have demonstrated incredible versatility, from producing massive amounts of energy required to power a country to creating a variety of plastic materials. Canada contains approximately 23.8 billion cubic meters of oil reserves trapped in the form of oil sands, the third largest reserve in the world [1], [2]. Canadians have extensively researched and expanded the fields of oil sands extraction and refining, as well as dedicated considerable time to treating its byproducts. This chapter provides a comprehensive assessment of the methodology and current literature regarding oil sands operations in Alberta, Canada.

1.1 Oil Sands

1.1.1 Oil Sands Reserves in Alberta

Oil sands can be defined as sedimentary deposits that contains a viscous petroleum product, crude bitumen, blended with various minerals. Most of the crude bitumen found in Canada is located in Alberta in three main areas: Athabasca Wabiskaw-McMurray, Cold Lake Clearwater, and Peace River Bluesky-Gething. Together, these reserves account for an area of nearly 142,000 km^2 [3]. This encompasses about 20% of the surface area of Alberta (662,000 km^2) and is larger than the surface area of England (130,000 km^2). Figure 1.1 shows these three main areas.

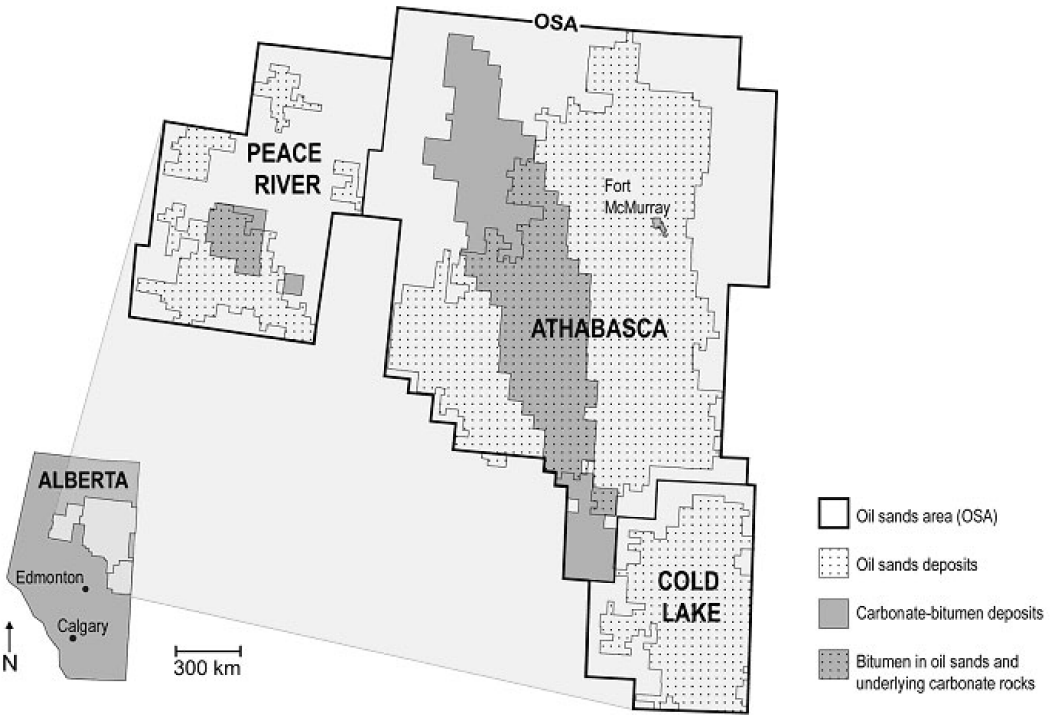

Figure 1.1: General area of the oil sands reserves in Northern Alberta, adapted from Hein, Marsh, and Bobby [4].

The most prevalent theory on the formation of oil sands is based on a sequence of steps that took place in geological time. First, dead marine life forms settled to the ocean floor and were eventually covered by sediments. Afterwards, their remains were buried deeper and deeper on the ocean floor. The resulting increasing pressure led to increased temperatures that helped convert

the organic matter (proteins, carbohydrates, etc.) into kerogen [1] which natural gas and petroleum are formed from. Meanwhile, the organic-rich sediments were transformed into rock. Finally, liquid petroleum began to flow through the pores of the rock, eventually forming oil reserves [3].

Crude bitumen is very viscous as a result of the bacteria-facilitated biodegradation of liquid petroleum. Over millions of years, this degradation formed heavy (high molecular mass) oil products that comprise crude bitumen. In addition, these crude bitumen reserves also have concentrations of heavy metals, complex sulphur- and nitrogen-based compounds that are higher than in conventional crude oils found elsewhere (Figure 1.2).

Figure 1.2: Photo of bitumen-rich oil sands during excavation [6].

1.1.2 Bitumen Extraction

In Alberta, two main methods are used to extract bitumen: surface mining and in-situ extraction.

When the oil sands ore is within 75 meters of the surface, the ore is most commonly extracted by surface mining. Four distinct layers must be considered during mining operations: muskeg, overburden, oil sands ore, and lime-

[1] Kerogen is defined as all insoluble sedimentary organic matter that includes both organic matter dispersed in sedimentary rocks as well as in pure organic deposits such as asphaltic substances and insoluble organic matter [5].

stone or granite [7]. The muskeg is the top layer of wet peatland that lies on top of the overburden. The overburden is a layer of sand and clay that carries less than <7 wt% bitumen. The oil sands ore is located under the overburden. The ore may contain anywhere from 7 to 14 % bitumen and is the desired product during the mining operation. Once the ore is mined, the bitumen is separated by the Clark hot water extraction process. It is estimated that approximately 20 % of bitumen reserves are recoverable by surface mining, whereas the remaining 80 % is recoverable by in-situ methods [8].

The Clark hot water extraction process was created by Dr. Karl Clark and his colleagues from the Research Council of Alberta, paving the way for modern large-scale bitumen extraction processes [3], [9]. In this process, the mined oil sands are mixed with hot water and other additives to liberate bitumen from sand and clay particles as froth. This froth is skimmed off to collect the bitumen, while the remaining sand/clay/water mixture (tailings) is sent to ponds.

Most oil reserves in Alberta are beyond the 75 m threshold and cannot be extracted via surface mining (Table 1.1). In-situ methods such as steam assisted gravity drainage (SAGD) are used to extract bitumen from these reserves. SAGD operates by inserting two parallel horizontal pipes into the oil sand reserve. The upper pipe releases steam to separate the bitumen from the sand and clay particles. The bitumen moves downwards via gravity into the secondary pipe that transports the liberated bitumen to the surface (Figure 1.3). This extraction process is less environmentally invasive and does not produce nearly as much solids waste as the surface mining method. Despite these advantages, surface mining has been practiced for decades because it is the easiest, most cost effective method.

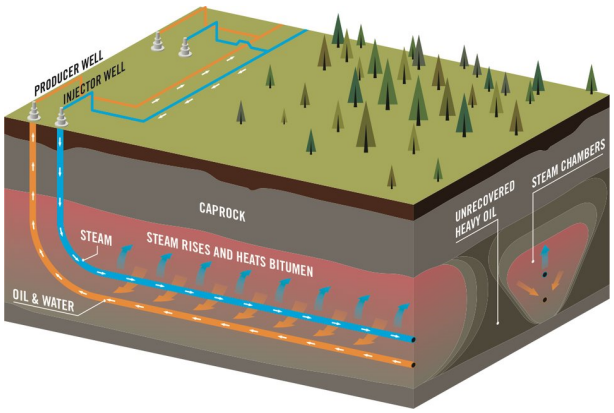

Figure 1.3: Drawing of SAGD process, adapted from JWN Energy [10].

1.1.3 Oil Sands Tailings

The solids waste stream of the Clark hot water extraction process (tailings) is a mixture of sand, clays, water, and some residual bitumen. The most common method to handle tailings is to transfer them to large excavated areas, such as abandoned mine sites or man-made dykes (tailings ponds, Figure 1.4). The goal is to allow the sand and clay particles to settle by gravity to the bottom of these basins, and reuse the supernatant water in the extraction process. The overall volume of tailings ponds is predicted to exceed 1 billion cubic meters in 2020 [11]. This volume is equivalent to the volume of 400,000 olympic-size swimming pools.

Table 1.1: Summary of estimated in-place and established mineable and in-situ bitumen reserves in Alberta as of 2014 [8].

Recovery Method	Initial volume in place (10^9 m^3)	Initial established reserves (10^9 m^3)	Remaining established reserves (10^9 m^3)
Mineable	20.8	6.16	5.16
In-situ	272.3	21.94	21.27
Total	293.1 (1 845 10^9 bbl)	28.09 (176.8 10^9 bbl)	26.43 (166.3 10^9 bbl)

Tailings ponds may be classified into three regions. The top layer is comprised of the supernatant water that can be recycled to the bitumen extraction process. Underneath it, is the fluid fine tailings layer (FFT), consisting of fine

clay particles with a less than 15 % overall solids content. After years, the fine particles from the FFT layer settle even more and form a sludge-like layer known as the mature fine tailings (MFT) layer, typically containing approximately 30 % solids. The MFT layer is troublesome: it forms a stable colloidal suspension that may take decades to centuries to settle by gravity.

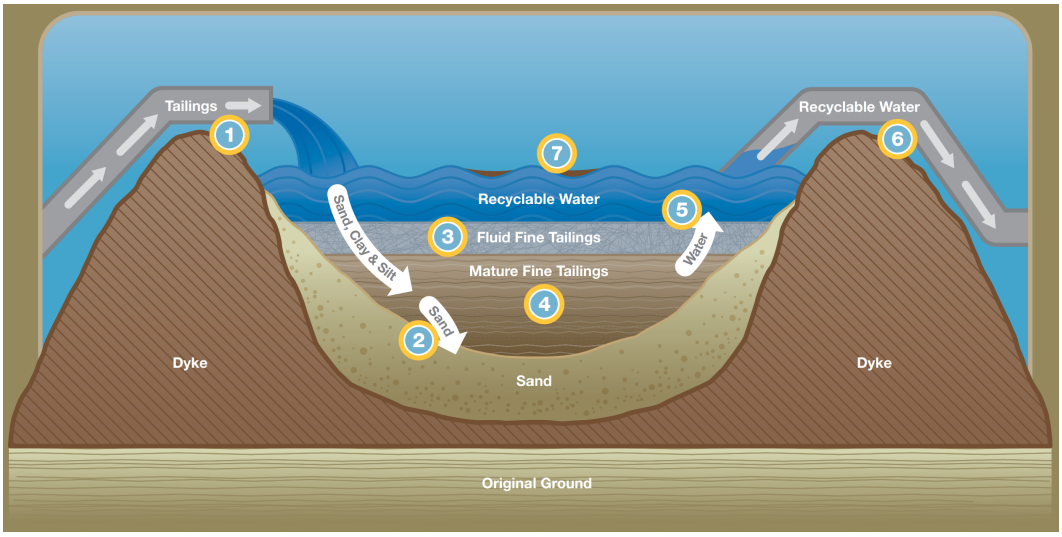

Figure 1.4: General schematic of tailings pond regions, adapted from the Government of Alberta [12].

The clays most typically found in oil sands samples are kaolinite, illite, chlorite, and montmorillionite. Several factors contribute to the stability of clays in water. Fine clays (with characteristic dimensions lower than 44 µm) are too small to settle as fast as larger particles. Moreover, their electric charges prevent them from agglomerating and settling faster.

Table 1.2: Typical characteristics of clays in an oil sands formation [3].

Mineral	Kaolinite	Illite	Chlorite	Montmorillonite
Abundance (wt. %)	69	28	1	0.3
Type of structure	Two-layer (TO)	Three-layer (TOT)		
Isomorphic substitution	Low in T	High in T	Both in T and O	

Clay minerals are composed of two different layers: a silicon-oxygen tetra-

hedron sheet (T) and an aluminum-oxygen-hydroxyl octahedron sheet (O). The two layers are covalently bonded via oxygen atoms in the tetrahedron sheet. The different combinations of these layers form the variety of clay types seen in Figure 1.5 and Table 1.2. Although the T and O sheets are typically neutral, they carry net negative surface charges for three reasons: 1) unequal dissolution of lattice-forming ions, 2) hydrolysis of broken surfaces, and 3) isomorphic substitution of ions.

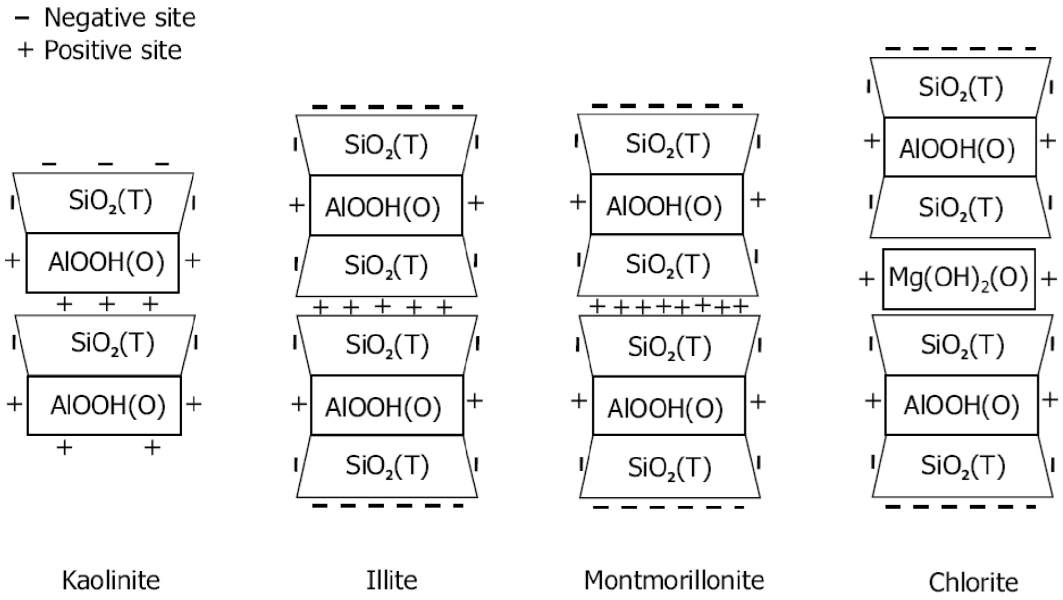

Figure 1.5: Clay structure and edge charges for kaolinite, illite, chlorite, and montmorillonite. Courtesy of Masliyah [3]

Isomorphic substitution is caused by high valence cations being replaced by lower valence cations (Si^{4+} with Al^{3+} in the T sheet and/or Al^{3+} with Mg^{2+}), which lead to permanent negative charges [13], [14]. The delamination of TO layers in kaolinite exposes the tetrahedron siloxane and aluminum hydroxyl surfaces (basal planes) to the surroundings, enabling them to undergo base hydrolysis. In addition to the basal planes, Si-O and Al-O bonds at the edges of the clay particles may also undergo hydrolysis. The bitumen extraction process is done at high pH to hydrolyze the siloxane groups and make them hydrophilic, which helps liberate bitumen [9], [15], [16]. Thus, clay particles in oil sands tailings typically have net negative surface charges.

1.1.4 Colloidal Stability of Clays in MFT

Surface electric charges and van der Waals forces are responsible for the colloidal stability of fine clay particles in MFT: surface charges lead to the formation of an electric double layer on the clay and water interface, while the small size of the clays make them subject to particle-particle interactions via van der Waals forces.

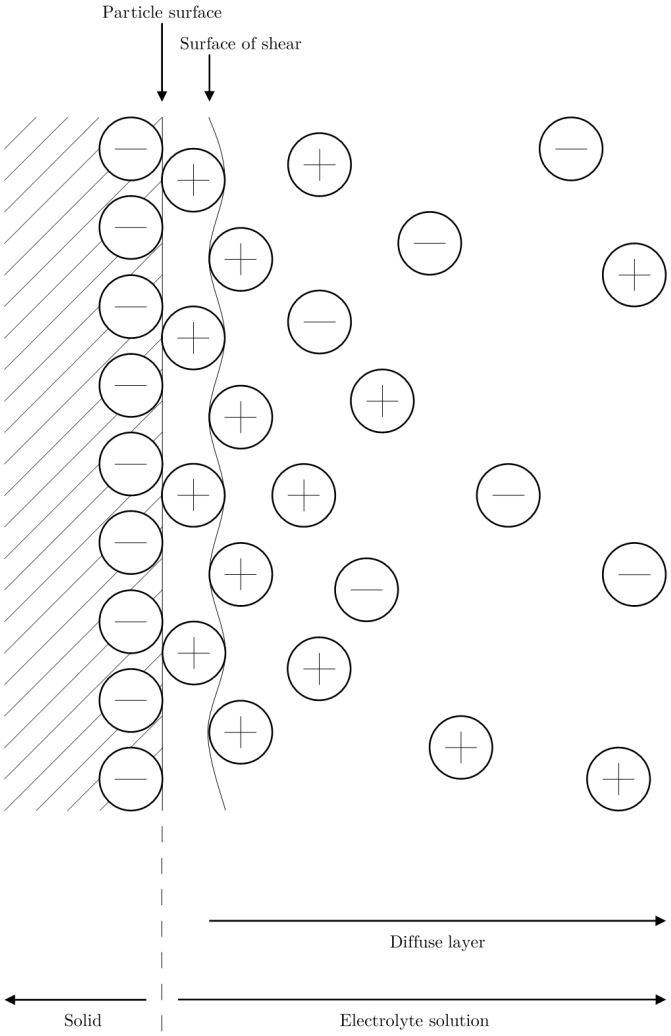

Figure 1.6: General schematic of an electric double layer [3].

As discussed in Section 1.1.3 various mechanisms are responsible for the formation of negative charges on the surface of clay particles. The resulting negative charges causes cations in solution to migrate to the clay surface to neutralize its negative charges, forming an electric double layer (Figure 1.8).

Tailings suspensions are subject to various electrokinetic phenomena (electrophoresis, sedimentation potential, streaming potential, and electro-osmosis) [3], [17]. The charges of the particles make them repel each other and avoid coagulation.

The electric double layer is not responsible solely for the stability of colloidal suspensions. Russian scientists Derjaguin and Landau, and Dutch scientists Verwey and Overbeek (DLVO Theory), first proposed that the total surface energy (E) in a colloidal suspension resulted from the combination of van der Waals attraction forces (E_{vdw}) and repulsive electric double layer forces (E_{dl}) [18], [19].

$$E = E_{vdw} + E_{dl} \tag{1.1}$$

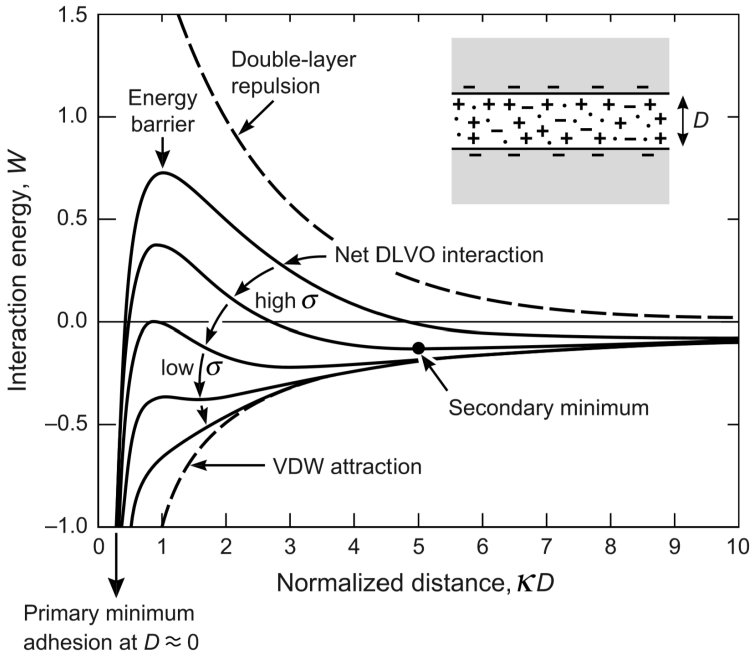

Figure 1.7: Plot of total energy (with varying surface potentials), van der Waals energy, and electric double layer energy of a typical colloidal solution from Israelachvili [20].

The resulting net energy is plotted as a function of the separation distance in Figure 1.7. In systems with high surface energy, a significant energy barrier and a secondary minimum are observed. The energy barrier results from the strong repulsion among the particles, which keeps them from aggregating. The secondary minimum occurs at the distance where the double layer repulsion

begins to decrease and the van der Waals force creates a subtle attraction, forming weak doublets with other particles [3].

1.1.5 Current State of Tailings Treatment

Many techniques are used to consolidate oil sands tailings into more manageable forms. The goal of most tailings treatments is to destabilize and compact the clay particles so that the solids and water can be separated. Some techniques to separate solids from water include centrifugation, filtration, and the addition of water-soluble polymer flocculants.

Centrifugation uses centripetal forces to promote particle aggregation. One of the most common types of centrifuges used in tailings treatment is the decanter centrifuge (Figure 1.8) [21]. This centrifuge contains a conveyor to transport the solids towards a conical beach, where they are discharged as a cake. The separated liquid is transported to the opposite end of the centrifuge. The resulting solids content of a typical MFT sample increases from about 30 % to approximately 60 % in this process.

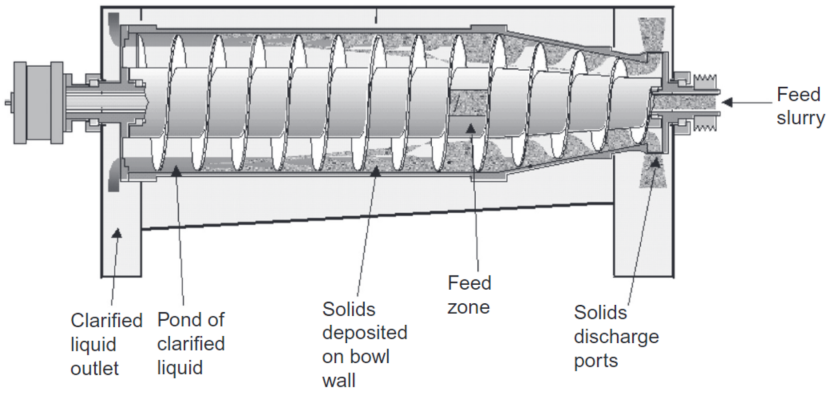

Figure 1.8: Schematic of a horizontal decanter centrifuge [22].

Another technique used to further dewater tailings is pressure filtration. In this method, the tailings sample is loaded into a chamber with a filter at the bottom. The chamber is then sealed and pressurized, forcing the liquid in the tailings through the interstitial voids of the filter cake (Figure 1.9). Filtration yields a dense filter cake and clarified water. Filtering performance is often evaluated by measuring the specific resistance of filtration (SRF) of

the tailings sample.

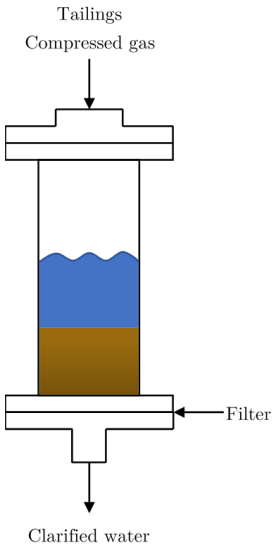

Figure 1.9: General diagram of a typical filtration unit.

In a typical filtration procedure, the SRF of the sample can be determined from the plot of filtration time divided by filtrate volume versus the filtrate volume:

$$SRF = \frac{2pA^2b}{c\mu} \tag{1.2}$$

where p is the pressure in kPa, A is the cross sectional area of the filter unit in m^2, b is the slope of the filtration time divided by the filtrate volume versus the filtrate volume in $^{s}/_{m^6}$, c is the suspension density in $^{kg}/_{m^3}$, and μ is the viscosity of filtrate in $Pa \cdot s$.

The SRF indirectly quantifies the radii of the capillary channels in the filter cake and the filter cake porosity [3], [11]. The greater the resistance in the tailings sample, the greater the amount of fine particles blocking capillary channels and inhibiting water from flowing through the cake. Thus, filtration is a practical choice for tailings samples with low fines content.

Flocculation, opposed to coagulation, uses water soluble polymers designed to overcome the stabilizing forces discussed in Section 1.1.4. Flocculants are used in many industries, such as adhesives, paints, paper, and water treatment because they alter the stability of heterogeneous mixtures. Thus, water-soluble

polymers are suitable candidates for the treatment of tailings. Considerable work has been done to enhance their performance [1], [2], [23]–[28].

1.2 Water Soluble Polymer Flocculants

Polymers are the product of the covalent bonding of many small, individual molecules, called monomers. Through various mechanisms, these monomers can be chemically bonded together to form chains of different lengths and configurations. This section focuses on the synthesis and application of water-soluble polymers for treating tailings.

1.2.1 Flocculation Mechanisms

Flocculation is a result of the destabilization of colloids via the reduction of repulsive forces. The addition of water-soluble polymer flocculants to a tailings sample effectively separates the water and clay particles by forming large clay aggregates (flocs). Polymer adsorbs onto the surface of clays and bring them closer together such that the particles are within the secondary minimum (as seen in Figure 1.7), allowing for flocculation to occur.

Typical polymer flocculants are long (with molecular weights in the order of millions of Daltons) and flexible chains. They need to be evenly dispersed within the suspension, be able to diffuse to the solid surfaces, adsorb on them effectively, and bridge the solid particles together via loops and tails (Figure 1.10) [3], [29]–[31].

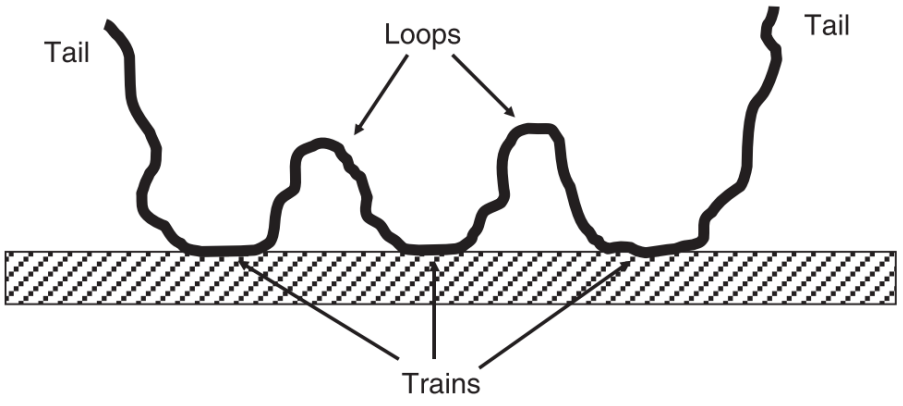

Figure 1.10: Loops and tails of a polymer adsorbed onto a solid surface, from Gregory and Barany [31].

The electrostatic charges of a polymer affect their adsorption onto solid surfaces. In addition to weak van der Waals attraction forces, neutral polymers

such as polyacrylamide (PAM), can interact via hydrogen bonds with surface silanol groups, leading to efficient flocculation. PAM is a popular flocculant for MFT treatment primarily because its chains are very long and flocculate clays efficiently [1], [2], [23]–[28]. Long polymer chains can attach to multiple sites on the solid surface and bridge several solid particles through loops and tails to create large flocs that precipitate fast.

Polyelectrolytes are subject to the same mechanisms as neutral polymers, but their electric charges alter how they adsorb on clay surfaces (Figure 1.11). A cationic polymer, for example will be attracted to the negatively charged surfaces of the clay particles (charge neutralization mechanism). The primary mechanism for anionic polymers varies slightly from that of cationic polymers. In this case, multi-valent counter-ions assist the flocculation by creating cationic "patches" and destabilizing the electric double layer (with greater valency resulting in greater destabilization according to the Schuzle-Hardy rule [32]). Anionic polymers neutralize patches of localized cationic charges resulting from the addition of multivalent ions, leading to charge-patch neutralization.

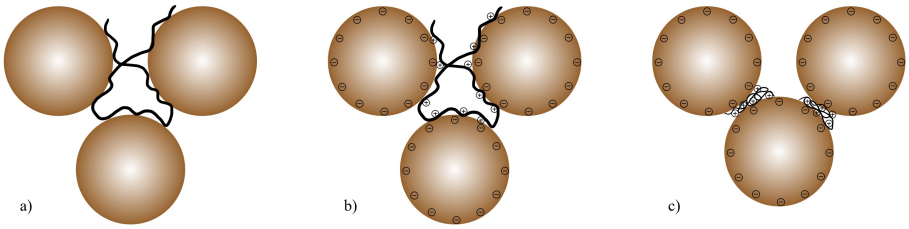

Figure 1.11: Mechanisms of clay particle flocculation: a) Bridging, b) Charge neutralization, c) Charge patch neutralization.

Figure 1.12 illustrates the different ways in which polymers may interact with solid surfaces. Interestingly, electrostatic attraction forces between cationic polyelectrolytes and negatively-charged clays may also have a negative effect, since charge density plays a significant role in the polymer conformation on the solid surface. Polymers with high charge density may adsorb almost completely on the surface (Figure 1.12b) and not form loops or trains. Contrarily, Figure 1.12c shows what may happen when the polymer does not interact so strongly with the clay surface. In the worst case scenario, the polymer

re-stabilizes the clay particles in the colloidal suspension via polymer overdose (Figure 1.12e).

Significant research has been dedicated to modify polymers properties to improve their flocculation efficiencies. The performance of PAM, for example, is considered to be optimal when its anionic charge is approximately 30 % to suppress hydrogen bonding effects [24], [33]–[35]. Modifications can range anywhere from synthesizing copolymers and terpolymers [36], controlling polymer dispersity, hydrolyzing functional groups for controlled hydrophobicity, and making graft hybrid copolymers, among other approaches.

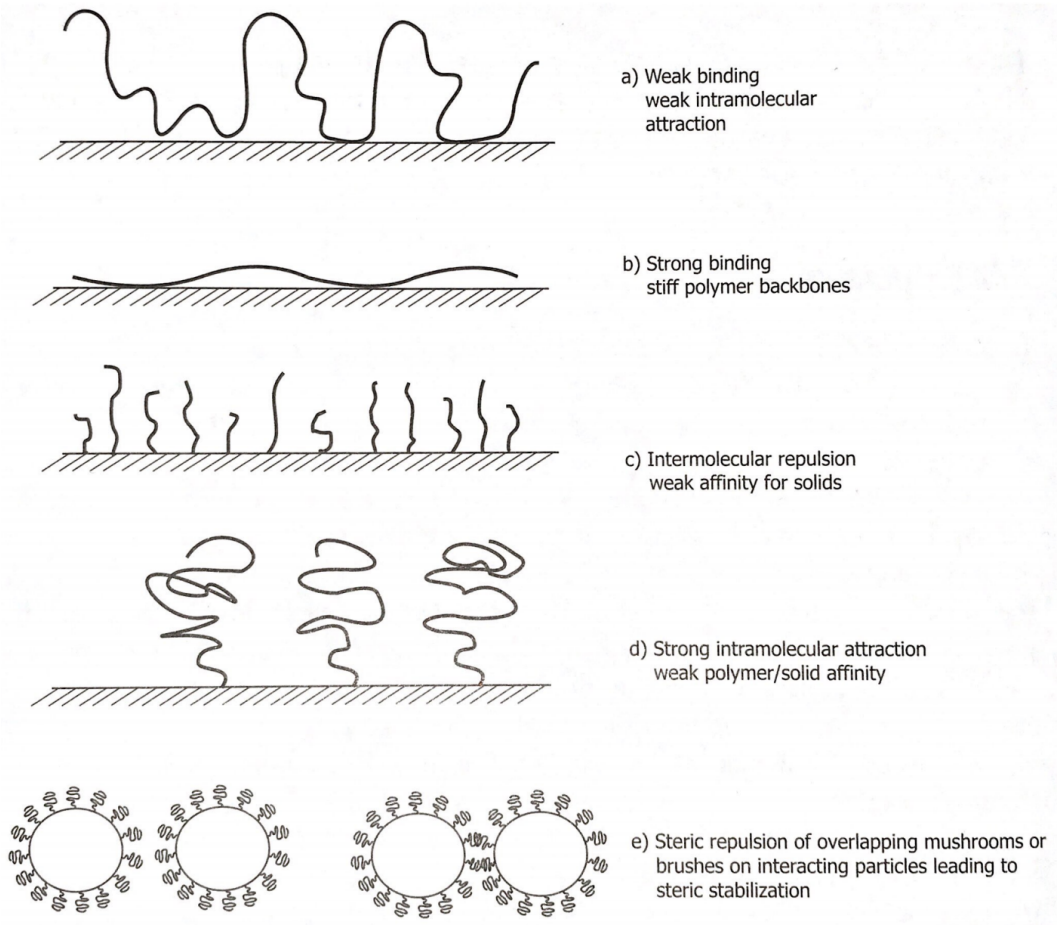

Figure 1.12: Various types of polymer adsorption on surfaces, from Masliyah [3].

1.2.2 Polymer Structure

Branched polymers have been used as effective MFT flocculants [1], [24], but a rigorous study on the effect of changing the degree of branching has yet to be performed.

In this thesis, I synthesized linear, 3-arm star, and 4-arm star homopolymers with approximately the same molecular weight and compared their flocculation and dewatering performances using a MFT sample. My main intent was to make polymers with precisely controlled molecular structures, so that the only main difference between them was their number of branches. This is the only unequivocal way to investigate the fundamental aspects of polymer topology on flocculation performance.

The method used to make these polymers needed to be reliable and precise, maintaining a constant growth of all polymer chains so that the arms of the star polymers had equal lengths. Conventional free radical polymerization was ruled out because it is a statistical polymerization mechanism that makes polymer chains with a wide distribution of sizes. Instead, I selected a controlled free radical polymerization technique called *atom transfer radical polymerization* (ATRP) because it can make linear and branched polymer chains with nearly the same length.

Atom transfer radical polymerization can make polymers with low dispersities due to its negligible termination rates.[2] This means that all polymer chains grow simultaneously at approximately the same rate and do not stop growing until the end of the polymerization. Assuming that all polymer chains start growing at about the same time, all of them will reach the same length after a given polymerization time. Therefore, ATRP can be used to make linear, 3-arm, and 4-arm star polymers of the same molecular weight. An overview of ATRP is discussed in detail in Section 1.3.

[2]The dispersity of a polymer measures how broad its distribution of chain length is. All chains have the same length in a polymer population with dispersity of 1.0. This is a limiting value never encountered in practice, but the closer to 1.0, the narrower the size distribution of the polymer population.

1.3 Polymer Synthesis

Polymers can be synthesized via many mechanisms. In this thesis, ATRP was chosen because it makes polymers with precisely controlled microstructures. Even though conventional free radical polymerization is less expensive, because it makes polymers with a statistical distribution of molecular weights and branching frequencies, it would not make polymers with the precision required to accurately compare the effects of branching in the flocculation and dewatering of MFT.

In free radical polymerization, the living polymer chains (polymer radicals) are rapidly terminated by combination or disproportionation, while other chains are being initiated in the reactor, forming polymers with a wide distribution of chain lengths (with minimum theoretical dispersities from 1.5 to 2.0). Contrarily, in ATRP the number of polymer chains is equal to the number of initiator molecules and chain termination is suppressed. As a result, polymers produced by ATRP have a significantly narrower distribution of chain lengths than those made with free radical polymerization.

1.3.1 Atom Transfer Radical Polymerization

In 1995, both Mitsuo Sawamoto and Krzysztof Matyjaszewski were credited with the discovery of atom transfer radical polymerization (ATRP) [37], [38]. ATRP is considered a controlled "living" chain growth polymerization mechanism because it can accurately control molecular weight, composition, and morphology of polymers by substantially reducing the frequency of chain termination and transfer events. The term "living", however has been discouraged by IUPAC because it is impossible to completely eliminate termination reactions between polymer radicals. Instead, IUPAC recommends the term controlled reversible-deactivation radical polymerization (RDRP) to describe ATRP [39].

ATRP differs from conventional free radical polymerization in several different ways. First, an alkyl halide (typically represented as **R-X**, where **R** is an alkyl group and **X** is a halide such as Cl or Br) and a transition metal

complex (**Mt^{n}X/L**, where **Mt** is a transition metal such as Fe, Cu, or Ru, **n** is its oxidation state, and **L** is a ligand) that behaves as a catalyst are required. A dynamic equilibrium between dormant alkyl halide species and polymer radicals is maintained to keep the polymerization under control (Figure 1.13). The reaction is slow, as ATRP is designed to push the equilibrium towards the dormant (left) side to avoid bimolecular polymer radical termination events (forming the dead chain **P-P** in Figure 1.13).

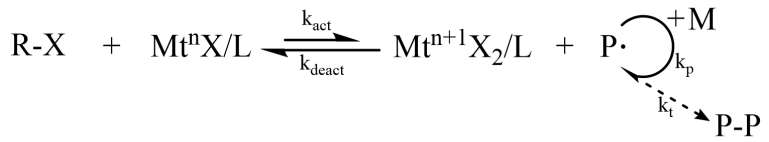

Figure 1.13: General scheme of atom transfer radical polymerization. (**R-X**: initiator or polymer chain (**P-X**) capped with a halide atom **X** (dormant state), **Mt^{n}**: transition metal complex with oxidation state **n**, **L**: ligand, **P·**: polymer radical, **M**: monomer), **P-P**: dead polymer chain.

In the ATRP process that is used in this thesis, the polymerization starts by contacting the initiator (**I-Cl**) and catalyst (**Cu^{I}Cl/L**) in its lower oxidation state, **n**, in the presence of the monomer, **M**. The catalyst abstracts the halide from the initiator molecule, increasing its oxidation state to **n+1** (**Cu^{II}Cl$_2$/L**) and generating a primary free radical initiator,

$$\mathrm{I{-}Cl} + \mathrm{Cu^{I}Cl/L} \underset{\mathrm{k'_{deact}}}{\overset{\mathrm{k'_{act}}}{\rightleftharpoons}} \mathrm{I}\cdot + \mathrm{Cu^{II}Cl_2/L} \tag{1.3}$$

The primary radical produced in this reaction, $\mathrm{I}\cdot$, can initiate the polymerization of monomer *M*, similarly to what happens in conventional free radical polymerization,

$$\mathrm{I}\cdot + \mathrm{M} \xrightarrow{\mathrm{k_i}} \mathrm{P_1}\cdot \tag{1.4}$$

The formed polymer radical keeps reacting with other monomer molecules in subsequent propagation reactions,

$$\mathrm{P}_i\cdot + \mathrm{M} \xrightarrow{\mathrm{k_p}} \mathrm{P}_{i+1}\cdot \tag{1.5}$$

where the subscript i is the number of monomeric units (chain length) added to the polymer radical.

In conventional free radical polymerization, bimolecular termination reactions will eventually stop the growth of the polymer radical molecules by combination or disproportionation, respectively,

$$\mathrm{P}_i\cdot + \mathrm{P}_j\cdot \xrightarrow{\mathrm{k_{tc}}} \mathrm{P}_{i+j} \tag{1.6}$$

$$\mathrm{P}_i\cdot + \mathrm{P}_j\cdot \xrightarrow{\mathrm{k_{td}}} \mathrm{P}_i + \mathrm{P}_j \tag{1.7}$$

resulting in the production of polymers with broad molecular weight distribution. In ATRP, however, the frequency of these termination steps is drastically reduced because polymer radicals will preferentially react with catalyst molecules in their **n+1** oxidation state, generating a dormant species, $\mathrm{P_n}$-X, that cannot terminate (or propagate),

$$\mathrm{P}_n{-}\mathrm{Cl} + \mathrm{Cu^{I}Cl/L} \underset{\mathrm{k_{deact}}}{\overset{\mathrm{k_{act}}}{\rightleftharpoons}} \mathrm{P}_n\cdot + \mathrm{Cu^{II}Cl_2/L} \tag{1.8}$$

Therefore, the key to reducing the frequency of polymer radical termination in ATRP is to push the equilibrium towards the dormant species (left side) and reduce the concentration of active polymer radicals in the reactor at any given time. This unique feature of ATRP is what reduces polymer dispersity values,

$$Đ = \frac{M_w}{M_n} \tag{1.9}$$

where M_n is the number average molecular weight and M_w is the weight average molecular weight. For conventional free radical polymerizations carried out at steady state under reactor uniform conditions, Đ varies from 1.5 (pure combination) to 2.0 (pure disproportionation). In ATRP, on the other hand, Đ reach values close to 1.0.

The "living" nature of ATRP is reflected in its first order polymerization kinetics behaviour, in which polymer molecular weight increases linearly with conversion according to the equation,

$$\mathrm{DP} = \frac{[M]_0}{[I]_0} \times X \tag{1.10}$$

where $[M]_0$ is the initial monomer concentration, $[I]_0$ is the initial initiator concentration, and X is the monomer conversion.

The rate of polymerization in ATRP in a batch reactor is given by the expression,

$$R_p = -\frac{d[M[}{dt} = k_p[M][P\cdot] \tag{1.11}$$

Assuming that initiation is fast and that the concentration of polymer radicals is constant, this equation can be easily integrated,

$$-\int_{[M]_0}^{[M]} \frac{d[M]}{[M]} = k_p[P\cdot]\int_0^t dt \tag{1.12}$$

$$\ln\frac{[M]_0}{[M]} = k_p[P\cdot]t \tag{1.13}$$

where k_p is the propagation constant.

Figure 1.14 is the semilog plot of $\ln {}^{[M]_0}/_{[M]}$ vs time. The plot is linear when the concentration of polymer radicals $[P\cdot]$ is constant. A positive curvature indicates that the concentration of polymer radicals increases during the polymerization, likely because of slow initiation rates. Contrarily, a negative curvature is a symptom of polymer radical termination events.

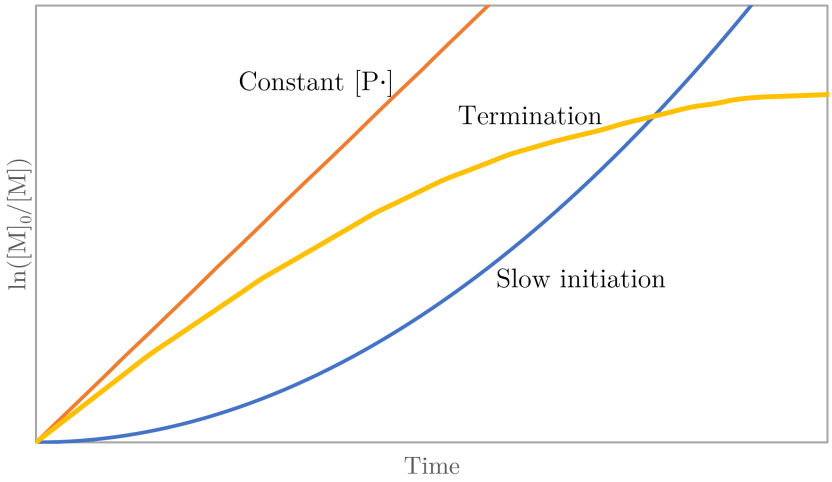

Figure 1.14: Variation of propagating radical species in ATRP [40].

Four conditions should be met to produce polymers with narrow dispersity [40]:

1. Fast rate of initiation (compared to the rate of propagation) to assure that most chains start growing at approximately the same time.
2. Fast exchange between species with different reactivities.

3. Propagation rate higher than depropagation rate.
4. Negligible chain transfer and termination rates.

Some of the disadvantages of ATRP are associated with the catalyst. Typically, ATRP requires a large concentration of catalyst to reach their target polymer molecular weight. The catalyst is also sensitive to impurities such as air, and catalyst removal from the polymer product is not trivial. ATRP catalysts are usually composed of metal halides and amine-based ligands which may be harmful. Solvent choices for ATRP are also quite limited. In addition, it is difficult to conduct ATRP in water because the halide ion, X, in the catalyst complex tends to dissociate due to the weak binding constant between Cu(II) and the halide [41]–[43] as shown below,

$$\mathrm{Cu/L} + 2\,\mathrm{Cl^-} \rightleftharpoons \mathrm{CuCl_2/L} \tag{1.14}$$

Recent advances in ATRP chemistry, however, have led to the development of modified ATRP processes, such as activators regenerated by electron transfer (ARGET) ATRP, initiators for continuous activator regeneration (ICAR), and supplemental activation reducing agent (SARA) ATRP, to name a few [41]–[45]. The following section will provide an overview of the ARGET ATRP technique, which is the method I used to make the polymers in this thesis.

1.3.2 Activators Regenerated by Electron Transfer ATRP

A few alternative ATRP techniques have been developed to address the challenges faced in traditional ATRP. The underlying mechanism of ATRP stays the same for these alternative methods, but the method of initiation varies among them [44]. ARGET ATRP, in particular, significantly reduces catalyst concentration to ppm amounts, better resist oxygen contamination, and make polymers of higher molecular weights (in the order of 1×10^6 g/mol). The key to this method is to introduce a reducing agent that regenerates the catalyst (activator) [41], [42], [46]–[49].

In addition to the mechanisms formulated in Equations (1.3) to (1.8), the

catalyst regeneration occurs simultaneously via the reaction,

$$\mathrm{RA}^{n+1} + \mathrm{Cu^{II}Cl_2}\,/\mathrm{L} \xrightarrow{k_{red}} \mathrm{RA}^{n} + \mathrm{Cu^{I}Cl/L} \tag{1.15}$$

where **RA** is the reducing agent.

In traditional ATRP, the Cu(II) catalyst may participate in side reactions (such as reacting with oxygen) that do not produce propagating species that form new chains [48]. However, we can add a reducing agent to regenerate the copper catalyst (reintroduce an electron) to enable it to form propagating species once again. This allows the polymerization to happen effectively with small catalyst concentrations (in the order of 10 ppm), making it easy to remove catalyst residues from the produced polymer.

Some reducing agents employed in ARGET ATRP reactions include ascorbic acid, tin(II) 2-ethylhexanoate, glucose (which are FDA approved substances) as well as hydrazine, solid silver, and solid copper [48], [50]–[56]. Figure 1.15 displays the overall scheme of an ARGET ATRP, where the most obvious difference from regular ATRP is the regeneration of the catalyst. In addition to the low concentration of catalyst, more eco-friendly solvents such as ethanol, water, and recently even untreated water (from the tap, rivers, rain, and ocean) have been used in these polymerizations [42], [47].

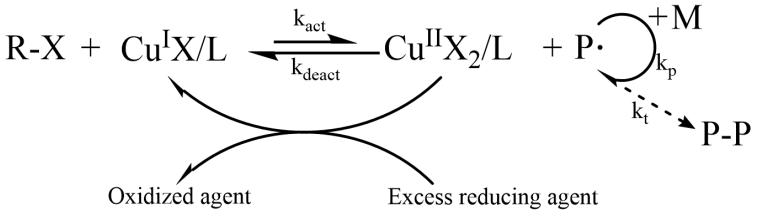

Figure 1.15: General reaction scheme of ARGET ATRP.

Although ARGET ATRP may be performed with small concentrations of catalyst, a closer inspection of the ATRP mechanism shows that the rate of polymerization is not directly proportional to catalyst concentration **Maty**,

$$R_p = k_p[P\cdot][M] = k_p K_{ATRP} \frac{[R-X][Cu^{I}X/L]}{[Cu^{II}X_2/L]}[M] \tag{1.16}$$

where K_{ATRP} is the ATRP equilibrium constant;

$$K_{ATRP} = \frac{k_{act}}{k_{deact}} \tag{1.17}$$

The rates of activation and deactivation are k_{act} and k_{deact}, respectively.

Equation 1.17 shows that the rate of polymerization is controlled not by the absolute catalyst concentration but rather by the ratio of Cu(I) to Cu(II) species $\frac{[Cu^{I}X/L]}{[Cu^{II}X_2/L]}$ [48], [57]. Therefore, it may be theoretically possible to reduce the concentration of catalyst to ppb level provided that this ratio is kept high. In reality, however, this is not a practical approach because of the unavoidable irreversible radical terminations that may occur in any polymerization. Furthermore, a sufficiently high concentration of the Cu(II) species is necessary for well defined and controlled ATRP reactions as per the equation for polymer dispersity in an ATRP reaction **Maty2**,

$$Đ = \frac{M_w}{M_n} = 1 + \left(\frac{k_p[R-X]}{k_{deact}[Cu^{II}X_2/L]}\right)\left(\frac{2}{X} - 1\right) \tag{1.18}$$

Chapter 2

Materials and Methods

This chapter describes the synthesis of linear, 3-arm star, and 4-arm star cationic poly((vinylbenzyl) trimethylammonium chloride) (L-PVB, S3-PVB, and S4-PVB, respectively), as well as the analyical techniques used to characterize them. The methods used to measure MFT flocculantion and dewatering efficiency will also be discussed in this chapter.

2.1 Materials

The monomer used for all polymerizations was (vinylbenzyl)trimethylammonium chloride (VB) (99 %, Sigma Aldrich). The ligand component of the catalyst was tris[2-(dimethylamino)ethyl]amine (Me_6TREN) (97 %, Sigma Aldrich), the transition metal component of the catalyst was copper (II) chloride (97 %, Sigma Aldrich), and the reducing agent used to supplement the catalyst was solid copper wire (99.9 %, 1mm diameter, Sigma Aldrich).

The initiator for the linear polymer was ethyl α-bromoisobutyrate (E-BiB) (98 %, Sigma Aldrich), the 3-arm star initiator was 1,1,1-tris(2-bromoisobutyryloxymethyl)ethane (3f-BiB) (97 %, Sigma Aldrich), and the initiator for the 4-arm star polymer was pentaerythritol tetrakis(2-bromoisobutyrate) (4f-BiB) (97 %, Sigma Aldrich).

The solvents used for the polymerizations were reagent alcohol (HPLC grade, 90 % ethanol, 5 % methanol, 5 % isopropanol, Sigma Aldrich), dimethyl sulfoxide (DMSO) (99.9 %, Sigma Aldrich), and deionized water. Acetone

(99.9 %, Sigma Aldrich) was used for the precipitation of the polymers.

2.2 Polymer Synthesis and Characterization

In this work, I used zero-valent copper as the reducing agent (solid copper wire) because it is easy to separate from the polymer and has essentially infinite reduction capability. Additionally, the use of copper wire allows for the precise control of catalyst regeneration. Simply removing the copper wire from the polymerization medium can effectively stop it by ending the regeneration of the catalyst from the deactivated state; placing it back in the reactor allows the polymerization to proceed, much like an on-off switch [58].

I also used a core-first approach to make the star polymers by selecting multifunctional ATRP initiators to ensure that the arms of each polymer star had approximately the same length (Figure 2.4).

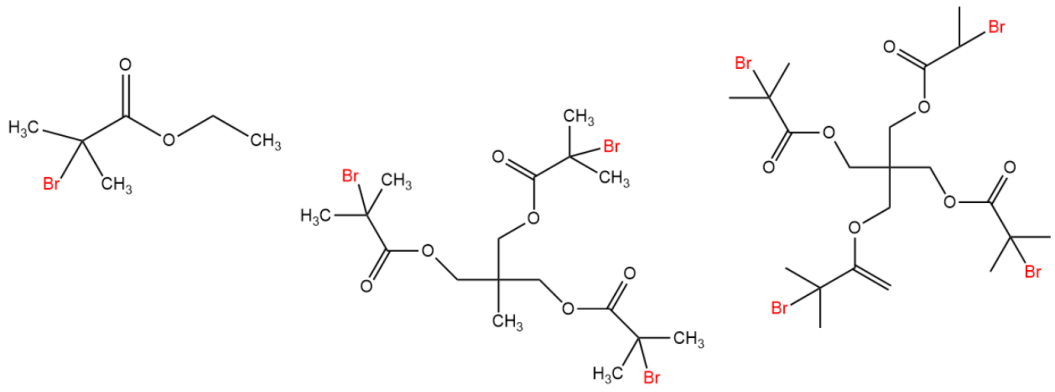

Figure 2.1: Mono, tri, and tetra-functional initiators used in this work to synthesize polymers of varying morphology via a core first approach.

A core first approach will ensure that the star polymer arms grow at the same rate as all other arms on the initiator. An arm first approach would not be ideal for this study because there is a possibility that the arms would not react with the multifunctional cores, which would lead to a blend of linear and star polymers in solution.

2.2.1 Synthesis of L-PVB

The monomer, VB, was dissolved in a 190 mL solution of deionized water. Copper wire was cut at an approximate length of 10 cm, and wrapped around a magnetic stir bar. The wrapped stir bar was then transferred to a solution of 1 M hydrochloric acid for a few minutes to remove any copper oxide from the wire surface. The wrapped bar was thoroughly rinsed with deionized water and added to the monomer solution. Next, copper (II) chloride and Me_6TREN were added to a 10 mL of deionized water, transferred to the monomer solution, which was then purged with nitrogen for approximately one hour. After purging, the mono-functional ATRP initiator, E-BiB, was added to the reaction mixture and the polymerization was allowed to proceed for approximately 4 days. Table 2.1 list the amounts of each reactant.

Table 2.1: Target mass and molar ratio of reactants used to make L-PVB

	VB	E-BiB	$CuCl_2$	Me_6TREN
Mass (mg)	24,894	1.53	1.58	5.42
Molar ratio	15,000	1	1.5	3.0

2.2.2 Synthesis of S3-PVB

The synthesis of S3-PVB followed a similar procedure to that used to make L-PVB, but the solvent was a 1:1 volume mixture of deionized water and reagent alcohol because the initiator was not soluble in pure water. The monomer was dissolved in a mixture of 90 mL deionized water and 100 mL reagent alcohol (90 % ethanol, 5 % methanol, and 5 % isopropanol). The remaining 10 mL of water were used to prepare the catalyst solution of copper (II) chloride and Me_6TREN, which was then added to the monomer solution and purged with nitrogen for approximately one hour. The tri-functional initiator, 3f-BiB, was prepared by first dissolving it in reagent alcohol and then added to the reaction mixture and left for 10 days. The amounts of each reactant are displayed Table 2.2.

Table 2.2: Target mass and molar ratio of reactants used in the ARGET ATRP of S3-PVB

	VB	3f-BiB	$CuCl_2$	Me_6TREN
Mass (mg)	22,128	2.96	2.108	6.02
Molar ratio	20,000	1	3.0	5.0

2.2.3 Synthesis of S4-PVB

The solvent used for this reaction was a mixture of 30 % DMSO and 70 % deionized water by volume due to the low solubility of 4f-BiB in pure water. The monomer was dissolved in 60 mL of DMSO and 130 mL of water. The remaining 10 mL was used to prepare the mixture of copper (II) chloride and Me_6TREN, which was added to the monomer solution. The tetra-functional initiator, 4f-BiB was dissolved in DMSO and added after purging the reactant mixture for one hour and left for 5 days. Table 2.3 contains the amounts of each reactant.

Table 2.3: Target mass and molar ratio of reactants used in the ARGET ATRP of S4-PVB

	VB	4f-BiB	$CuCl_2$	Me_6TREN
Mass (mg)	16,596	2.87	1.581	4.515
Molar ratio	20,000	1	3.0	5.0

2.2.4 Gel Permeation Chromatography

Molecular weights of the polymers were measured using an Agilent Technologies 1260 Infinity Gel Permeation Chromatograph/Size Exclusion Chromatograph (GPC/SEC) equipped with a triple detection system (refractive index, light scattering, and viscometer). The polymer was dissolved in an aqueous mobile phase with a concentration of 0.2 M NaCl and a pH of 3.30, with a polymer concentration of 3 $^{mg}/_{mL}$. Approximately 100 µL of polymer was injected at a flow rate of 1 $^{mL}/_{min}$ for 40 minutes at 30 °C.

2.3 MFT Treatment

The MFT sample was diluted to 5 wt. % in 100 mL solutions for testing. The MFT suspension is mixed for 2 minutes using a screw style impeller at 300 rpm prior to polymer addition. This impeller was created in a CAD program and 3D printed from polyethylene teraphthalate glycol. It was designed to have the same height of the MFT suspension and the same width of the beaker to ensure homogeneous mixing throughout the suspension[59]. As well, PVB is a shear sensitive polymer and the flocs are easily broken. The screw impeller applies the greatest homogeneous shear force throughout the whole solution, opposed to the standard pitch blade impellers commonly used in overhead mixing applications which have very high shear zones right at the impeller. The MFT-polymer solution was allowed to mix for one minute at 300 rpm. The following subsections details various metrics used to evaluate flocculant efficacy.

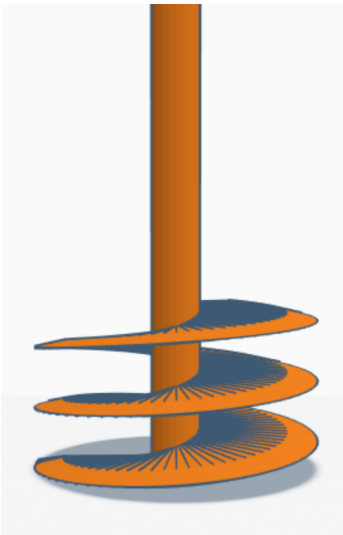

Figure 2.2: CAD render of auger impeller.

2.3.1 Initial Settling Rate

The flocculated MFT sample was poured into a 100 mL graduated cylinder, where the settling rate was measured over time. The settling of the MFT versus time was plotted versus time and the slope of the linear portion of the

settling rate was used to calculate the reported initial settling rate (ISR) value, as shown in Figure 2.3.

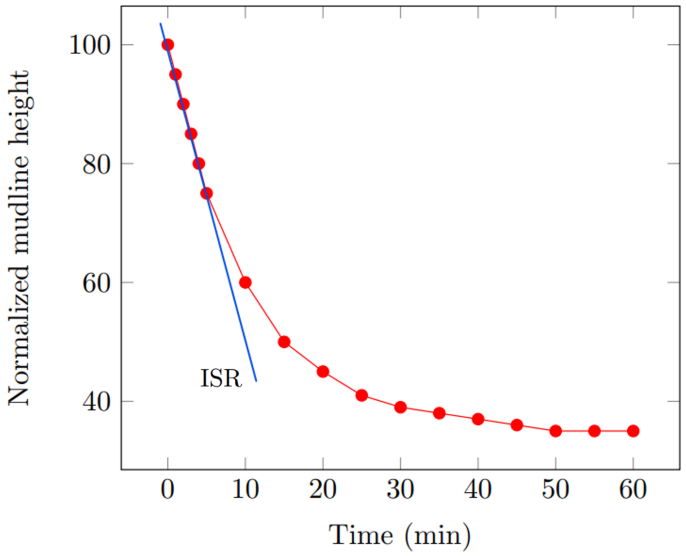

Figure 2.3: General methodology to determine ISR by the settling rate versus time graph.

2.3.2 Capillary Suction Time

Capillary suction time (CST) measures the time it takes for water to move through a 3 mL sample of the flocculated MFT immediately after mixing with the flocculant. A Type 319 Multi-Purpose CST from Triton Electronics (Figure 2.4) was used to measure the CST of the flocculated tailings.

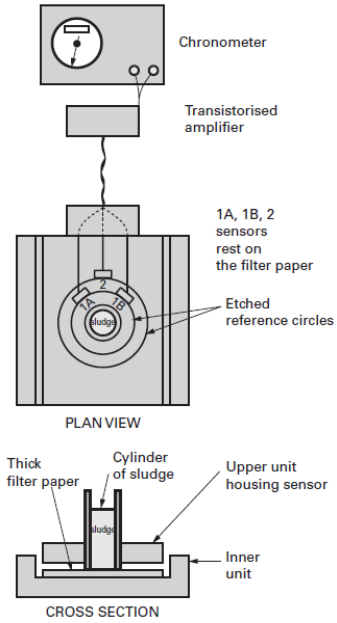

Figure 2.4: Schematic of a CST apparatus [60].

Chapter 3

Results and Discussion

3.1 Polymer Synthesis and Characterization

The following subsections outline the synthesis of L-PVB, S3-PVB, and S4-PVB. Each polymerization used either water, ethanol, DMSO, or their mixtures as solvents. Water is typically a challenging solvent to use in ATRP because it may dissociate the halide and catalyst complex as discussed in Section 1.3.1. The VB monomer, however, already contains a chloride ion that shifts the halide dissociation equilibrium to the right (product side) and helps maintain the catalyst in its proper form, as illustrated in Equation 1.14. [42], [43].

$$\mathrm{Cu/L} + 2\,\mathrm{Cl^-} \rightleftharpoons \mathrm{CuCl_2/L} \tag{1.14}$$

3.1.1 Synthesis of L-PVB

The concentration of unreacted monomer was calculated using the expression

$$[M] \times mw = \frac{[M]_0 \times V_s \times mw - m_{polymer}}{V_s} \tag{3.1}$$

where $[\mathrm{M}]_0$ is the initial molar concentration of monomer in the reactor, $\mathrm{V_s}$ is the volume of the aliquot, mw is the monomer molar mass, and $\mathrm{m_{polymer}}$ is the mass of polymer.

Therefore, [M] can be easily calculated as,

$$[M] = [M]_0 - \frac{m_{polymer}}{V_s \times mw} \tag{3.2}$$

The natural logarithm of the initial monomer concentration divided by the aliquot monomer concentration is plotted against time (the graphical representation of Equation 1.13) in Figure 3.1. The linear dependency indicates that the radical concentration was constant during the polymerization. This is a defining feature of ATRP and proves that the polymerizations took place according to our expectations [40].

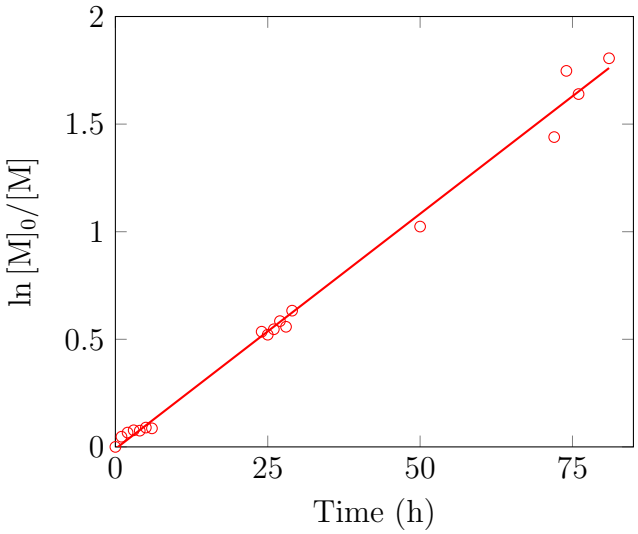

Figure 3.1: Dependency of $\ln [M]_0/[M]$ on time for the synthesis of L-PVB

Furthermore, Figure 3.2 illustrates qualitatively how the mass of polymer increased with polymerization time.

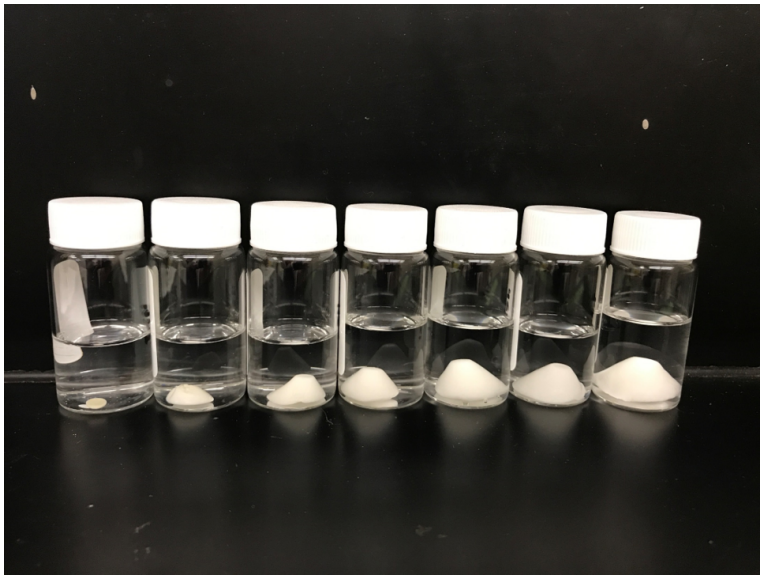

Figure 3.2: Increasing L-PVB mass over the span of the polymerization from 2 hours to 95 hours.

3.1.2 Synthesis of S3-PVB

The same sampling procedure used for L-PVB was repeated during the synthesis of S3-PVB over a span of approximately nine days. The linear trend in Figure 3.3 suggests a steady, constant growth of polymer chains expected in ATRP.

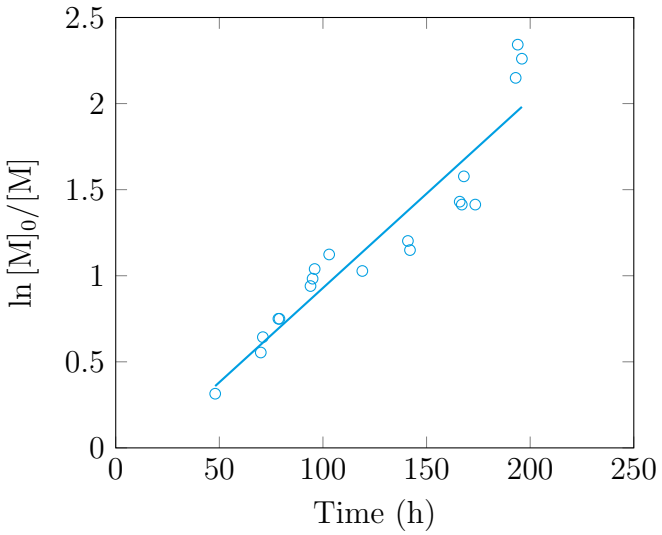

Figure 3.3: Dependency of $\ln [M]_0/[M]$ on time for the synthesis of S3-PVB.

3.1.3 Synthesis of S4-PVB

A similar polymerization procedure was followed for the synthesis of S4-PVB. Figure 3.4 shows that the linear trend that indicates constant chain growth was maintained for five days.

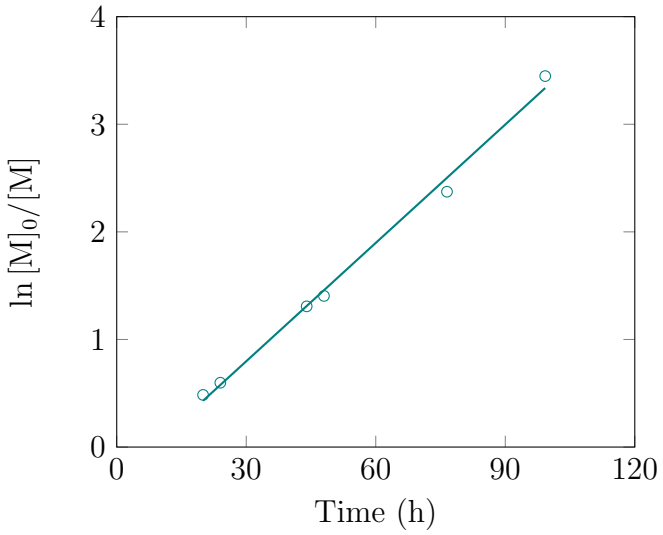

Figure 3.4: Dependency of $\ln [M]_0/[M]$ on time for the synthesis of S4-PVB.

3.1.4 Gel Permeation Chromatography

L-PVB

Table 3.1 lists some M_n values for L-PVB made at different polymerization times. The molecular weight increased steadily with time reaching high values up to 3 million Daltons. Perhaps more importantly, the dispersity remained low at about 1.2 proving that the controlled free-radical poylmerization was successful. Figure 3.5 shows that M_n also increased linearly with conversion, as expected for ATRP.

Table 3.1: Number average molecular weight, conversion, and dispersity of L-PVB at varying times

Time (h)	M_n (g/mol)	Conversion	Dispersity
28	1 489 000	0.08	1.23
50	2 143 000	0.64	1.19
72	2 166 000	0.76	1.21
95	2 976 000	0.89	1.19

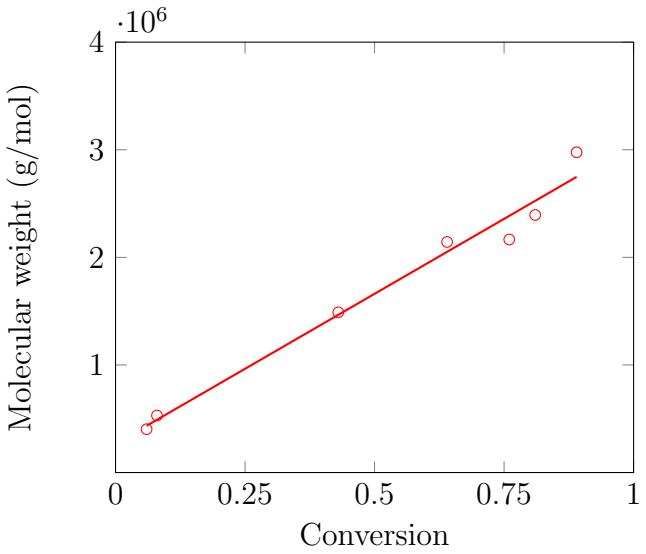

Figure 3.5: L-PVB molecular weight evolution as a function of conversion.

S3-PVB

Table 3.2 lists the M_n values, conversion, and dispersity for S3-PVB. This polymerization could also produce high molecular weight polymers with low dispersity values, likely because the ethanol present in the reaction medium decreased the rate of polymerization and thus increased the control of the polymerization. The evolution of molecular weight with conversion is shown in Figure 3.6. The molecular weight of the 3-arm star polymer also depended linearly on conversion.

Table 3.2: Number average molecular weight, conversion, and dispersity of S3-PVB at varying polymerization times.

Time (h)	M_n (g/mol)	Conversion	Dispersity
48	1 118 235	0.25	1.04
71	1 791 163	0.45	1.02
94	2 164 717	0.57	1.02
141	2 347 724	0.66	1.03
168	2 780 971	0.75	1.03
193	3 089 610	0.83	1.02
222.5	3 320 792	0.93	1.02

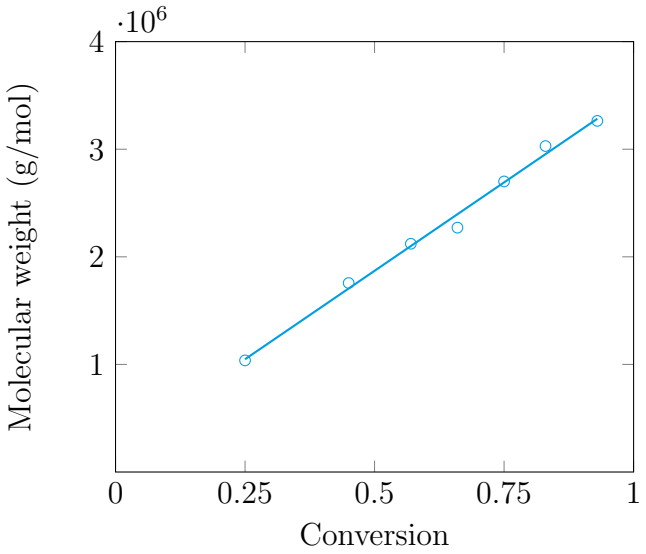

Figure 3.6: S3-PVB molecular weight evolution as a function of conversion

S4-PVB

The 4-arm star PVB was also made with high molecular weights and also low dispersities, as shown in Table 3.3. Similarly to the other two polymers, the molecular weights of S4-PVB depended linearly on conversion (Figure 3.7).

Table 3.3: Number average molecular weight, conversion, and dispersity of S4-PVB at varying polymerization times

Time (h)	M_n (g/mol)	Conversion	Dispersity
24	1 311 281	0.45	1.14
48	1 895 244	0.75	1.05
76.5	2 844 702	0.91	1.05
117.5	3 084 073	0.97	1.07

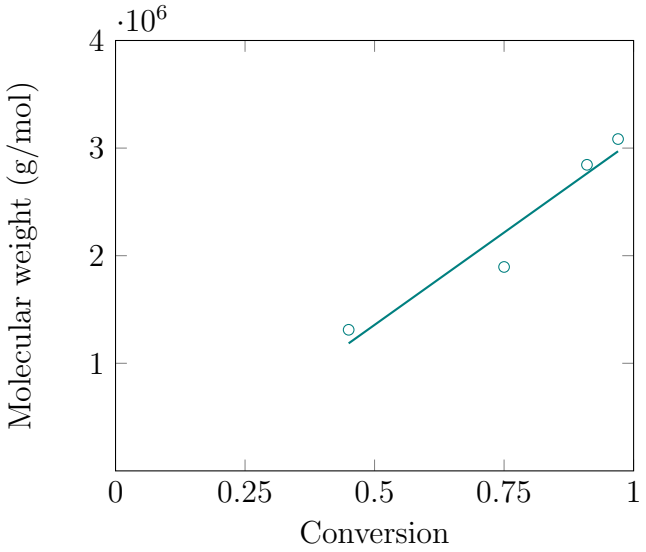

Figure 3.7: S4-PVB molecular weight evolution as a function of conversion

3.2 MFT Treatment

Polymers with approximately the same M_n (3 000 000 $^{g}/_{mol}$) were chosen to flocculate and dewater MFT to assess the differences between the linear, 3-arm, and 4-arm star configurations performance: L-PVB made after 95 hours, S3-PVB after 193 h, and S4-PVB after 117.5 hours.

3.2.1 Initial Settling Rate

L-PVB

Figure 3.8 shows how the normalized settling rates vary for different dosages of L-PVB. MFT settles slowly for a dosage of 3000 ppm, increases sharply when the dosage is raised to 5000 ppm, but then slows down when the dosage is further increased to 7000 and 9000 ppm, perhaps indicating polymer overdosing.

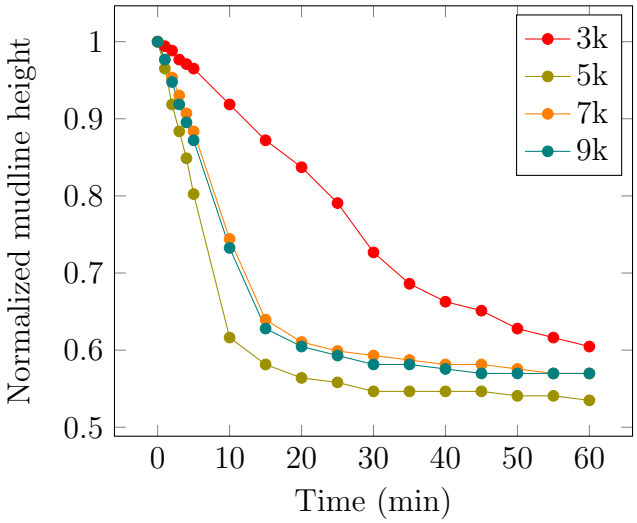

Figure 3.8: Normalized settling rates with L-PVB polymer series (dosages in 1000 ppm).

Figure 3.9 compares the pictures of the sedimentation cylinders after 24 hours of the sedimentation for all dosages. Mudline heights did not differ much among the different L-PVB dosages and the supernatant turbidity remained low in all cases.

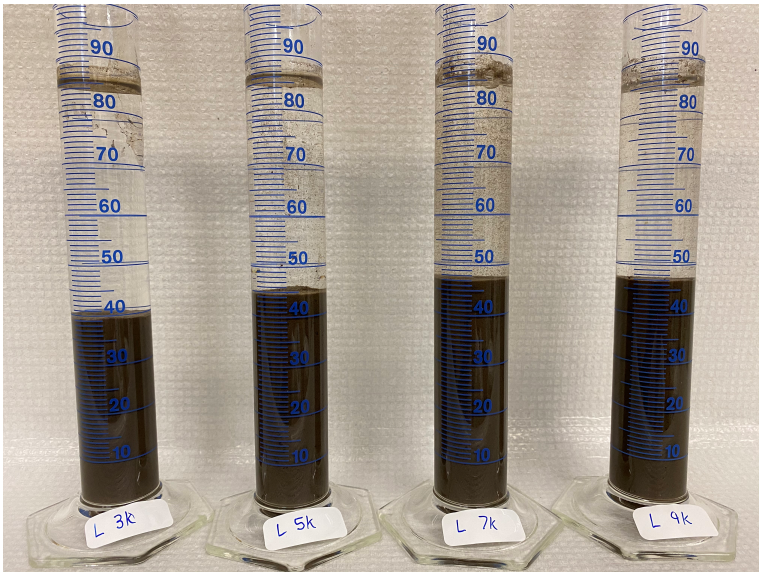

Figure 3.9: Effect of L-PVB dosages on MFT mudline height and supernatant turbidity.

S3-PVB

A graphical representation of the normalized settling rates of MFT with S3-PVB is seen in Figure 3.10. As for its linear counterpart, a dosage of 5000 ppm also led to the fastest settling rate with the 3-arm star polymer.

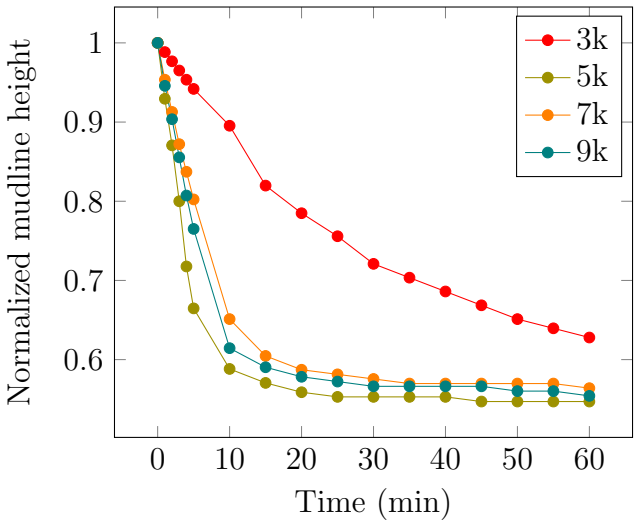

Figure 3.10: Normalized settling rates with S3-PVB (dosages in 1000 ppm).

The photo in Figure 3.11 indicates that the mudline level and supernatant turbidity did not vary much among different dosages of S3-PVB.

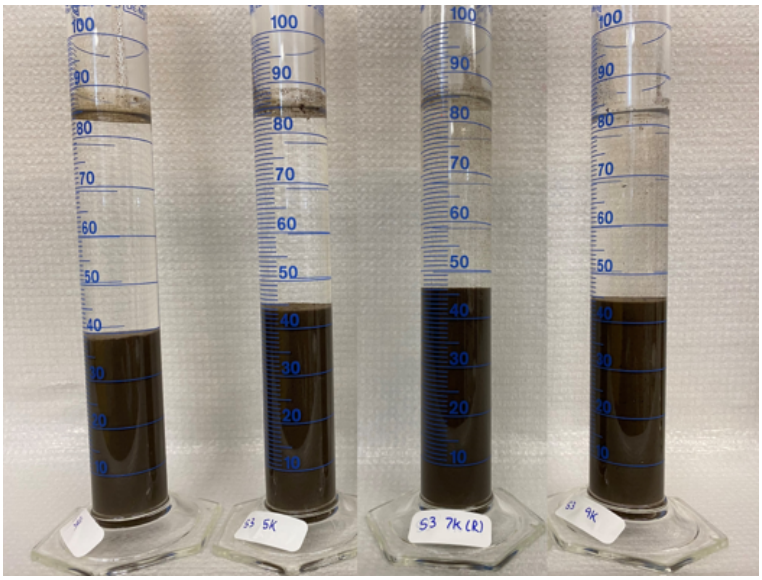

Figure 3.11: Effect of S3-PVB dosage on MFT mudline height and supernatant turbidity.

S4-PVB

Figure 3.12 shows that for dosages equal to or higher than 5000 ppm, the settling rates with S4-PVB remained practically the same, but that at 3000 ppm settling was quite slow. Interestingly, Figure 3.13 also shows that the supernatant turbidity for MFT treated with only 3000 ppm of S4-PVB was much higher than for any other test done in this investigation.

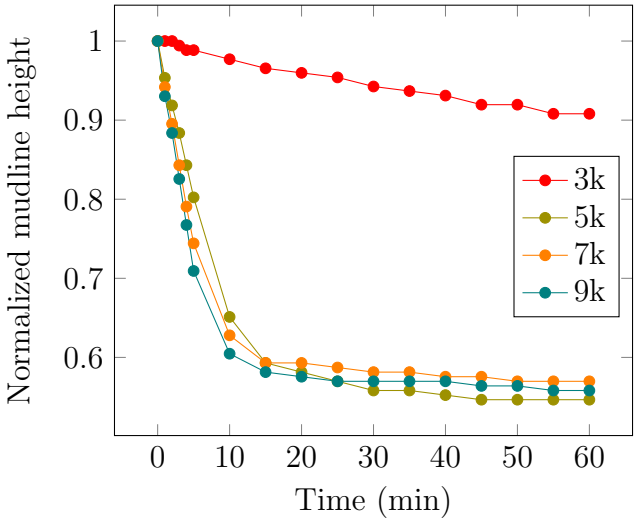

Figure 3.12: Normalized settling rates with S4-PVB (dosages in 1000 ppm).

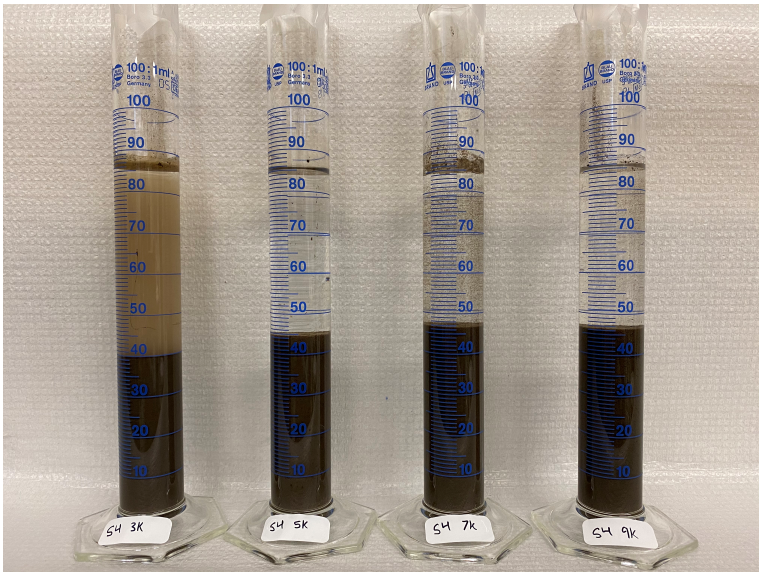

Figure 3.13: Flocculation series of S4-PVB.

Initial Settling Rate Summary

Figure 3.14 compares the initial settling rates (ISR) of the three polymers at different dosages. The ISR values were calculated by measuring the slopes of the initial linear regions of the normalized settling rate curves. S3-PVB outperformed L-PVB in all dosages, while S4-PVB only performed well at the highest dosages. A dosage of 5000 ppm for L-PVB and S3-PVB led to the highest ISRs and lowest relative turbidities (as seen in Figures 3.9 and 3.11). Furthermore, although the ISR for S4-PVB increased continuously with dosage, the supernatants had relatively higher turbidities, except for a dosage of 3000 ppm.

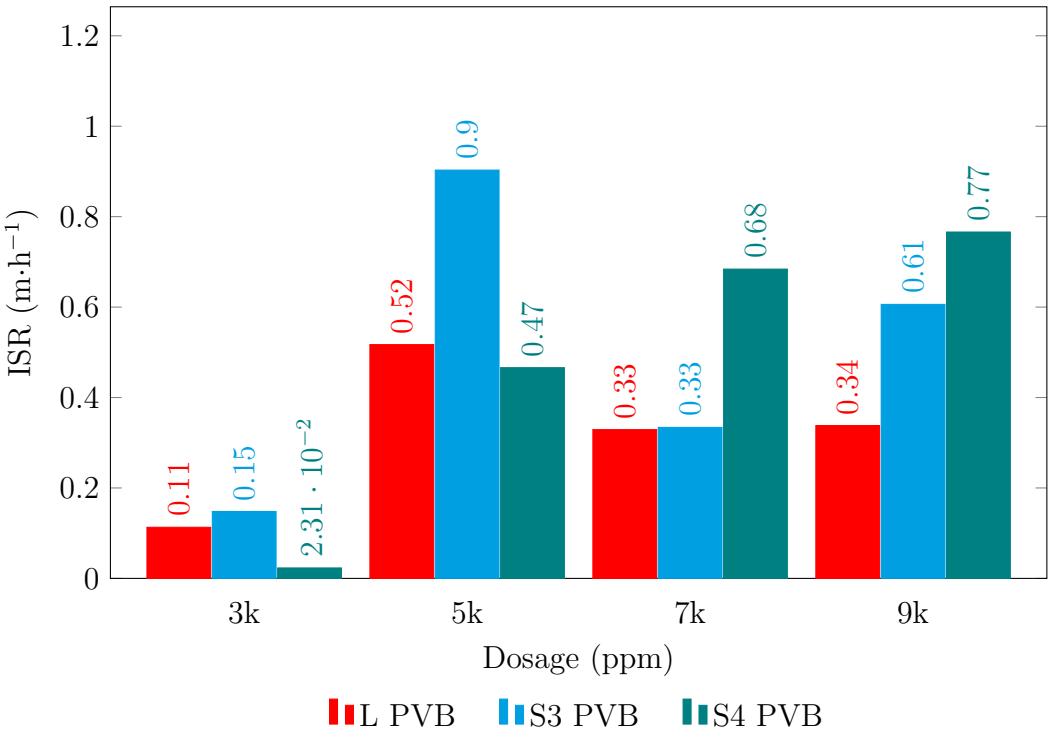

Figure 3.14: Initial settling rates for L-PVB, S3-PVB, and S4-PVB.

The 4-arm star polymer, S4-PVB, showed a distinct behaviour at its lowest dosage of 3000 ppm in terms of ISR, CST, and relative turbidity. An additional dosage range was tested from 2500 ppm to 4000 ppm to further observe this behaviour (Figure 3.15).

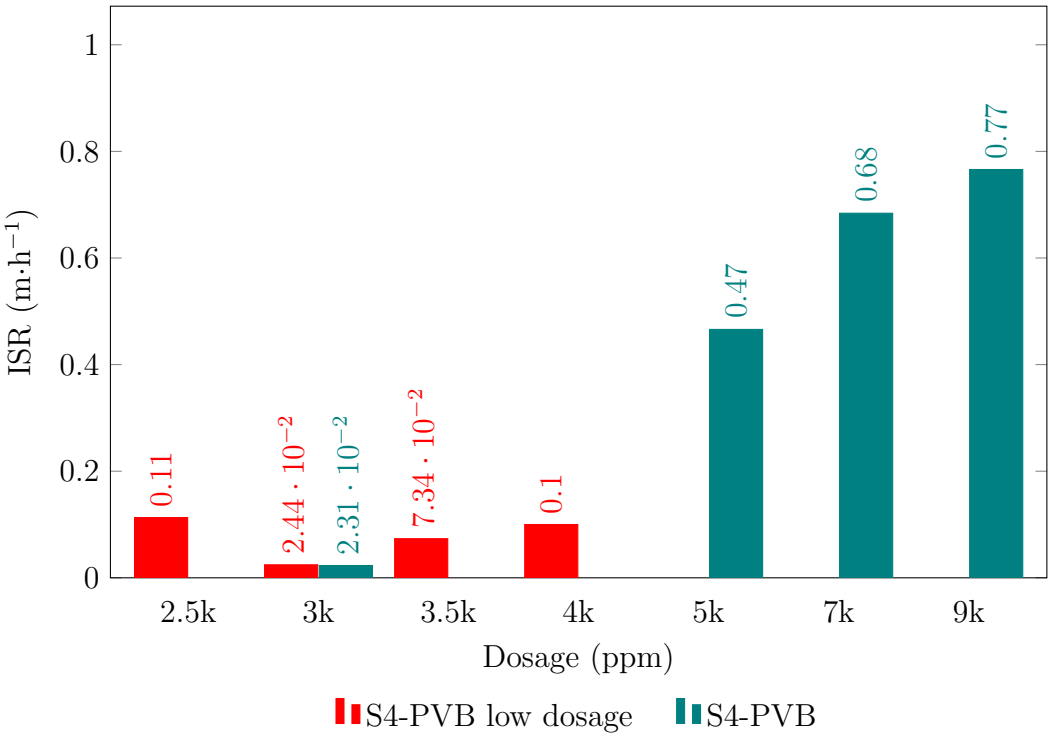

Figure 3.15: Initial settling rate values for S4-PVB over an extended dosage range.

Figure 3.15 shows that for dosages lower than or equal to 3000 ppm, S4-PVB did not perform well. One needs to increase it dosage to at least 5000 ppm for the performance of the 4-arm star to become similar to its linear or 3-arm analogue. It should be noted that although the ISR at a dosage of 2500 ppm was higher than at 3000 and 5000 ppm, this came with a much larger turbidity, as seen in Figure 3.17, indicating that the flocculation of the fine particles was inefficient and only the larger particles settled to the bottom of the cylinder.

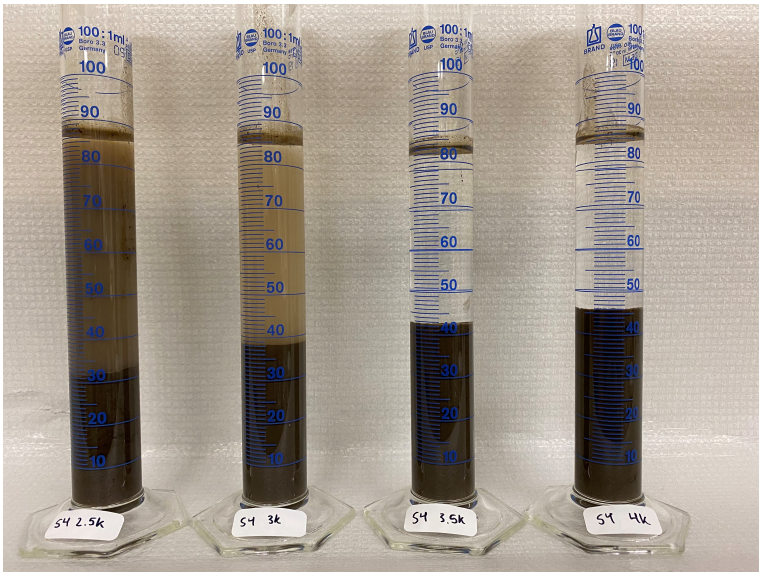

Figure 3.16: Low dosage flocculation experiments with S4-PVB.

3.2.2 Capillary Suction Time

Suspension CST Results

The suspension CST values were determined immediately after the MFT was flocculated. Both L-PVB and S3-PVB performed identically across the entire dosage range, while S4-PVB only performed on par with the other polymers beyond the 3000 ppm dosage, as shown in Figure 3.17. A possible explanation for this observation may be that the 4-arm star polymer has shorter arms than those of the 3-arm star and linear polymer of the same molecular weight. Consequently, its size in solution was also smaller and its arm extended out in solution for shorter distances, thus reaching fewer clay particles. When used at a low dosage, this may make this polymer an ineffective flocculant. In addition, because PVB is a cationic polymer, there may be some polymer stiffness as a result of steric interactions between charged arms stemming from the same center. This effect may not be as extreme in the 3-arm star polymer because the arms may be long enough to minimize this effect after some distance away from the core, but it may be more relevant for the 4-arm star. Furthermore, smaller flocs decrease the pore/void size between flocs which would negatively affect the de-waterability of the flocs.

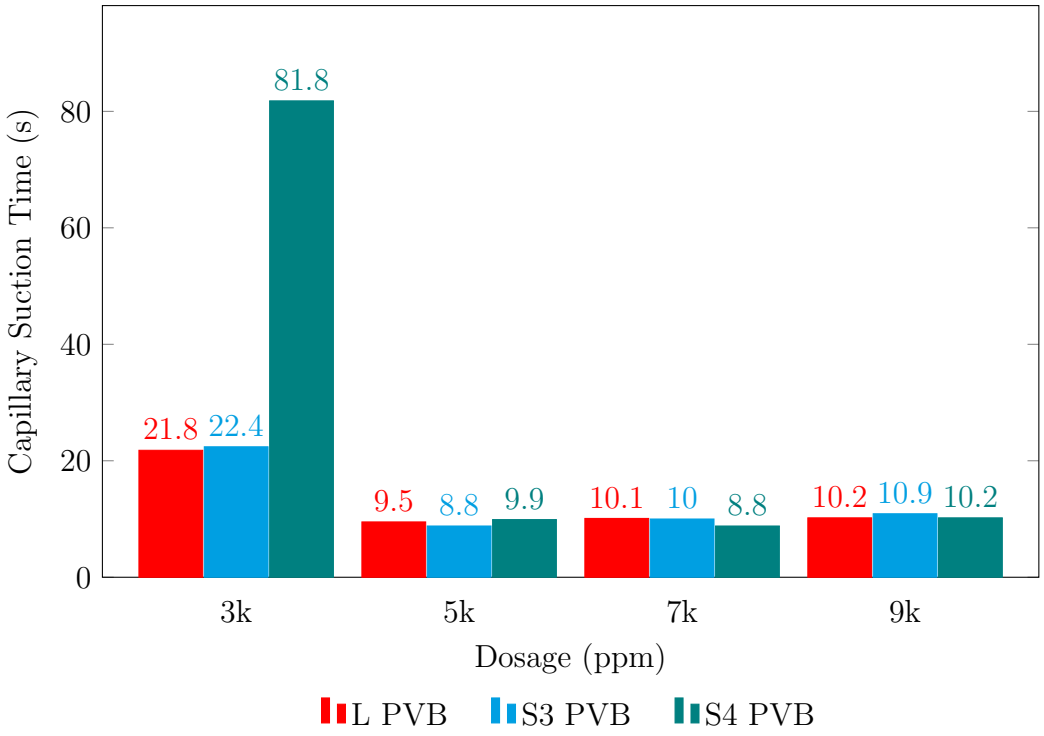

Figure 3.17: Suspension capillary suction times for L-PVB, S3-PVB, and S4-PVB.

A closer look at the extended S4-PVB dosage range shows the overall decrease of CST values with increasing polymer dosage, with the 9000 ppm increasing slightly, an indication of a polymer overdose (Figure 3.18). This verifies the deviation in performance that is observed in the low ppm range of S4-PVB when compared to the other PVB analogues.

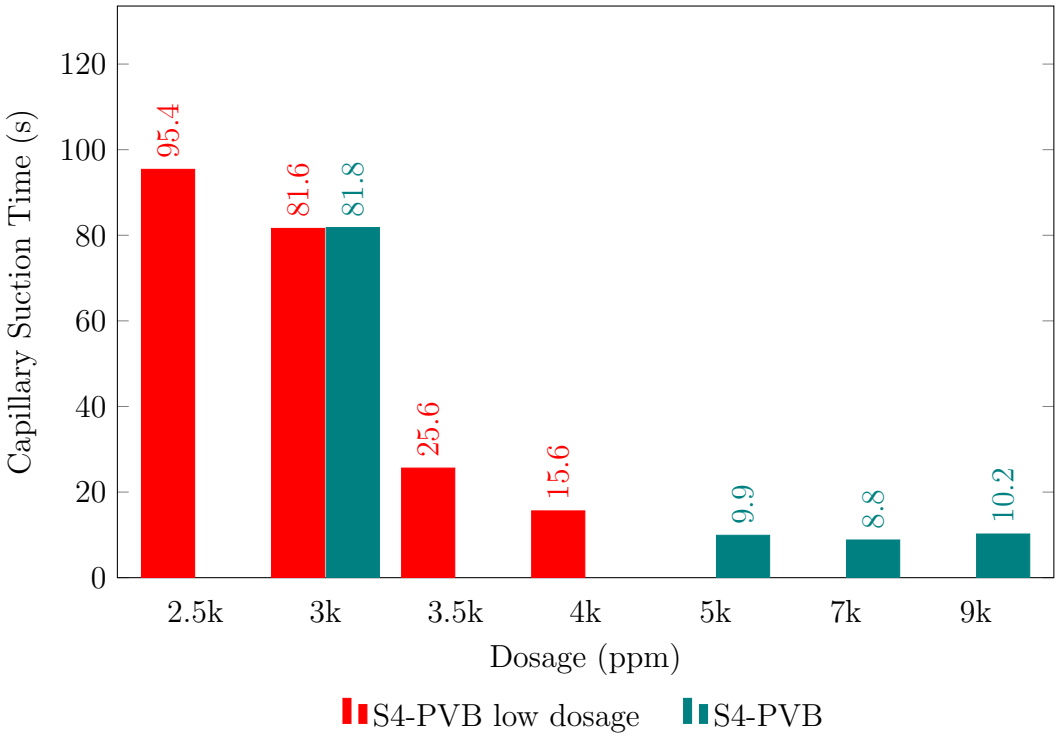

Figure 3.18: Capillary suction time values for S4-PVB over an extended dosage range.

Sediment CST Results

The same trend observed for the suspension CST was repeated when the CST of the sediments was measured. The only significant difference was that when a dosage of 3000 ppm was used, it took approximately twice as long to de-water the sediments than the suspension. This is not surprising, since the solids content in the sediments after 24 hours was about twice that in the suspension (Figure 3.19); solids that contain less water will naturally de-water at slower rates.

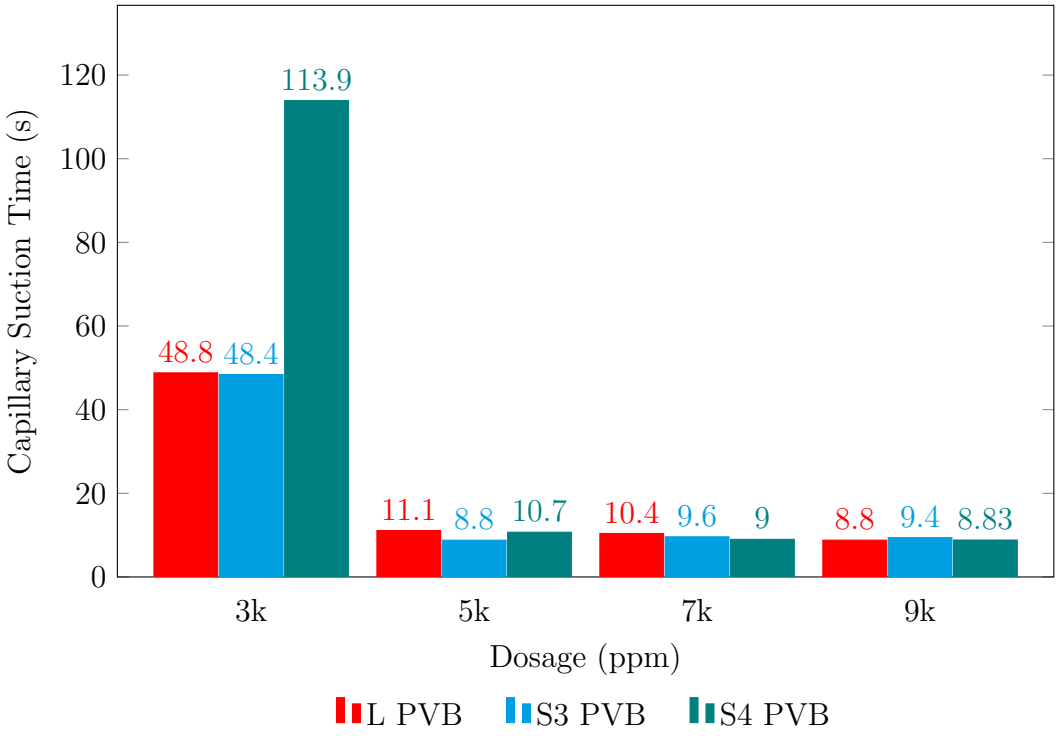

Figure 3.19: Sediment capillary suction times for L-PVB, S3-PVB, and S4-PVB.

The extended dosage range for S4-PVB followed the same trends (Figure 3.20), with increasing dosages leading to faster de-watering.

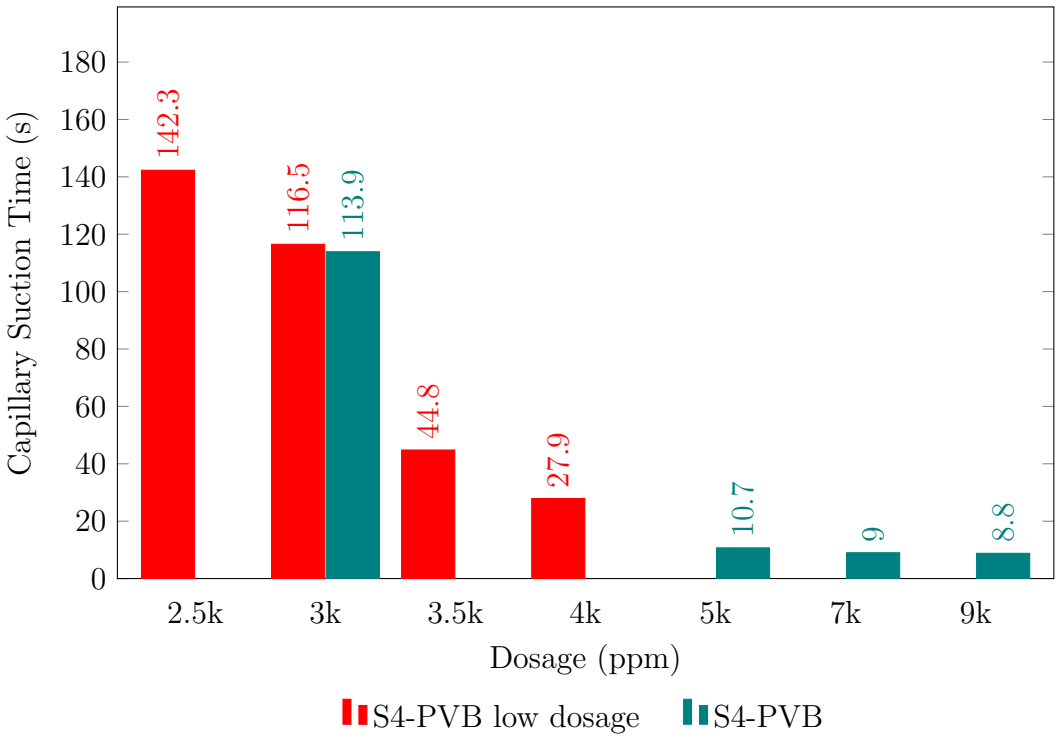

Figure 3.20: Sediment capillary suction times for the extended dosage range of S4-PVB.

3.2.3 Solids Content

Surprisingly, the solids content in the sediments was not substantially affected by polymer dosage or configuration (Figure 3.21). The main difference between solids contents across the polymer dosage range was that at the lowest 3000 ppm dose, the solids contents were about one or two percent greater than in the other dosages. This was likely due to the fact that the smaller flocs were able to compact to a greater degree than the other, larger flocs made at the other dosages. It is important to keep in mind that the turbidity of the supernantant at the 3000 ppm dosage was also higher, meaning that some of the fines remained suspended in this case. Otherwise, all the polymers seemed to perform relatively the same and doubled the approximate wt. % of the original MFT solution.

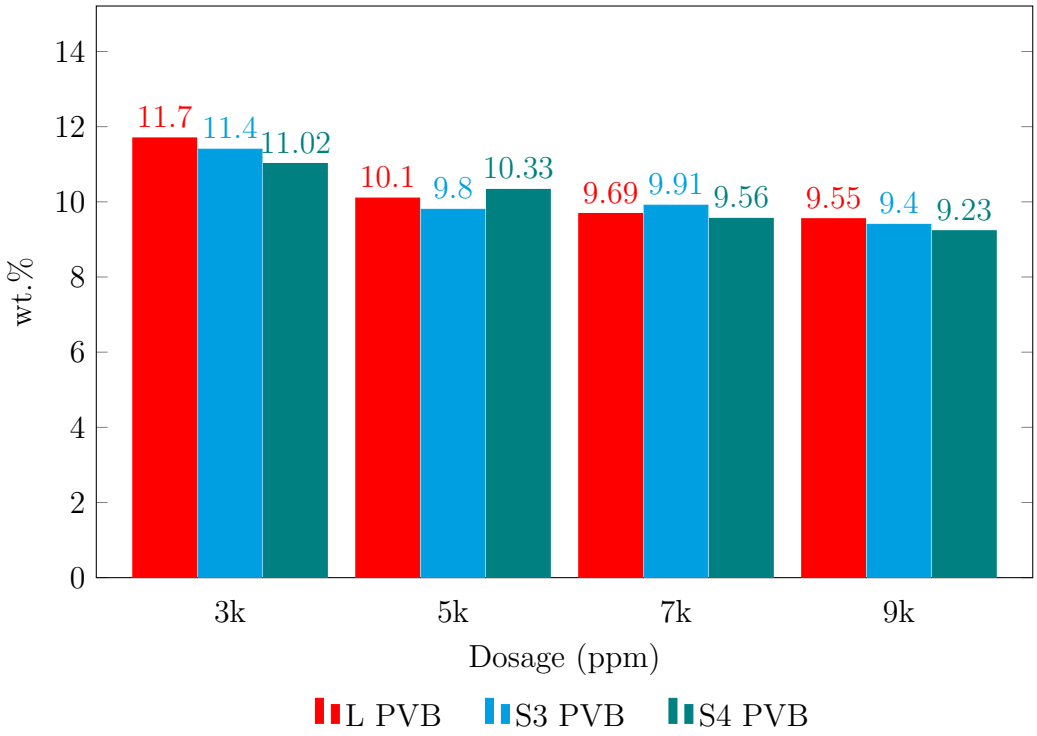

Figure 3.21: Solids content of MFT after 24 hours of flocculation with L-PVB, S3-PVB, and S4-PVB.

Chapter 4

Conclusions and Future Work

Three different morphologies (linear, 3-arm star, and 4-arm star) of poly(vinylbenzyl)trimethylammonium chloride) were successfully synthesized via ARGET ATRP with high molecular weights and narrow polymer dispersities in environmentally friendly solvents. Additionally, each polymerization used less than 50 ppm of catalyst.

The positive flocculation characteristics of PVB, fast de-waterability and clear supernatant, were maintained across the different polymer morphologies compared in this investigation. In the initial settling rate tests, the 3-arm star polymer (S3-PVB) outperformed the linear polymer (L-PVB) at every tested dosage, while the 4-arm star polymer (S4-PVB) was most effective at the two highest dosages (7000 and 9000 ppm).

The capillary suction time (CST) test was used to measure the dewaterability of the flocs formed with the three polymer analogues. L-PVB and S3-PVB per- formed nearly identically at every dosage in the suspension CST tests, while S4-PVB performed very poorly at the lowest tested dosage (2500 ppm). The sediment CST values followed similar trends to those of the suspension CST values, with the exception that the dewatering times were approximately twice as long for the 3000 ppm dosage.

The solids content after 24 hours showed very minimal variation between the three polymers tested. Overall, the polymer morphology seemed to have not affected the solids content of the MFT after flocculation.

In conclusion, it seems that branching morphology, at least for PVB, plays a

minor role on flocculation and de-watering of MFT, provided that all polymers have the same molecular weight.

Future Work

PVB can dewater MFT rapidly while also providing very clear turbidities. I have shown that PVB maintains these traits even when its linear configuration is changed to a 3 or 4-arm star configuration. Since branched polymers have lower viscosities (at the same molecular weight), it may be advantageous to treat MFTs with branched polymers that will have lower viscosities and will be easier to mix and disperse in the MFT suspension. Some future work that may be performed to extend the scope of this investigation include:

- Extend the degree of branching by using different star polymer cores.
- Use other monomers and/or comonomers to make star polymers to find out if the results for PVB also apply to them.
- Use ATRP to make well defined block (linear or branched) copolymers to find out its effect on MFT flocculation and de-watering.
- Since PVB is inherently shear sensitive, modify a natural polymer such as amylopectin (which is much more shear resistant) with an ATRP initiator. This would essentially create a highly branched molecule with precisely grafted arms.

References

[1] S. P. Gumfekar, V. Vajihinejad, and J. B. Soares, "Advanced Polymer Flocculants for Solid–Liquid Separation in Oil Sands Tailings," *Macromolecular Rapid Communications*, vol. 40, no. 1, pp. 1–18, 2019, ISSN: 15213927. DOI: 10.1002/marc.201800644. 1, 12, 14, 16

[2] D. R. Vedoy and J. B. Soares, "Water-soluble polymers for oil sands tailing treatment: A Review," *Canadian Journal of Chemical Engineering*, vol. 93, no. 5, pp. 888–904, 2015, ISSN: 1939019X. DOI: 10.1002/cjce.22129. 1, 12, 14

[3] J. H. Masliyah, J. Czarnecki, and Z. Xu, *Handbook on Theory and Practice of Bitumen Recovery from Athabasca Oil Sands Volume I: Theoretical Basis*. Kingsley Knowledge Publishing, 2011, ISBN: 978-1-926832-03-6. 2–4, 6–11, 13, 15

[4] B. F. Hein, R. Marsh, and M. Boddy, "Overview of the Oil Sands and Carbonate Bitumen of Alberta: Regional Geologic Framework and Influence of Salt-Dissolution Effects*," Tech. Rep., 2008. [Online]. Available: http://www.searchanddiscovery.com/documents/2008/08017hein/images/hein.pdf. 2

[5] M. Vandenbroucke and C. Largeau, "Kerogen origin, evolution and structure," *Organic Geochemistry*, vol. 38, no. 5, pp. 719–833, 2007, ISSN: 01466380. DOI: 10.1016/j.orggeochem.2007.01.001. 3

[6] S. McCarthy, *Why the oil sands matter to every Canadian - The Globe and Mail*. [Online]. Available: https://www.theglobeandmail.com/report-on-business/rob-magazine/why-the-oil-sands-matter-to-every-canadian/article21331322/?click=sf%7B%5C_%7Dglobe%7B%5C#%7Ddashboard/follows/. 3

[7] Oil Sands Magazine, *Surface Mining Techniques used in the Oil Sands — Oil Sands Magazine*. [Online]. Available: https://www.oilsandsmagazine.com/technical/mining/surface-mining. 4

[8] Alberta Energy Regulator, "ST98-2015: Alberta's energy reserves 2014 and supply/demand outlook 2015-2024," Tech. Rep., 2015, p. 299. 4, 5

[9] J. Masliyah, Z. J. Zhou, Z. Xu, J. Czarnecki, and H. Hamza, "Understanding Water-Based Bitumen Extraction," *Water*, vol. 82, no. August, pp. 628–654, 2004. 4, 7

[10] JWN Energy, *Temporarily shutting in oilsands SAGD wells might not be as harmful as you think — Oilsands & Heavy Oil — JWN Energy*. [Online]. Available: https://www.jwnenergy.com/article/2016/5/temporarily-shutting-oilsands-sagd-wells-might-not-be-harmful-you-think/. 5

[11] D. Vedoy, L. Botha, and J. Soares, "Filtering Mature Fine Tailings Flocculated with Single and Dual Anionic / Cationic Polymers," in *19th International Seminar on Paste and Thickened Tailings*, PASTE 2016, 2016, pp. 1–12. 5, 11

[12] Government of Alberta, "Environmental Management of Alberta's Oil Sands," Tech. Rep., 2009. 6

[13] H. Welfare, G. Sposito, N. T. Skipper, R. Sutton, S.-H. Park, A. K. Soper, and J. A. Greathouse, "Surface geochemistry of the clay minerals," *Proceedings of the National Academy of Sciences*, vol. 96, no. 7, pp. 3358–3364, 1999, ISSN: 0027-8424. DOI: 10.1073/pnas.96.7.3358. [Online]. Available: http://www.pnas.org/content/96/7/3358%7B%5C%%7D5Cnhttp://www.pnas.org/cgi/doi/10.1073/pnas.96.7.3358. 7

[14] P. Leroy and A. Revil, "A triple-layer model of the surface electrochemical properties of clay minerals," *Journal of Colloid and Interface Science*, vol. 270, no. 2, pp. 371–380, 2004, ISSN: 00219797. DOI: 10.1016/j.jcis.2003.08.007. 7

[15] S. Basu, K. Nandakumar, S. Lawrence, and J. Masliyah, "Effect of calcium ion and montmorillonite clay on bitumen displacement by water on a glass surface," *Fuel*, vol. 83, no. 1, pp. 17–22, 2004, ISSN: 00162361. DOI: 10.1016/S0016-2361(03)00222-9. 7

[16] J. Liu, Z. Xu, and J. Masliyah, "Interaction forces in bitumen extraction from oil sands," *Journal of Colloid and Interface Science*, vol. 287, no. 2, pp. 507–520, 2005, ISSN: 00219797. DOI: 10.1016/j.jcis.2005.02.037. 7

[17] J. H. Masliyah and S. Bhattacharjee, *Electrokinetic and Colloid Transport Phenomena*. John Wiley & Sons, Inc., 2006, ISBN: 9780471788829. 9

[18] B. Derjaguin and L. Landau, "Theory of the stability of strongly charged lyophobic sola dn of the adhesion of strongly charged particles in solutions of electrolytes," 1941. DOI: 10.1016/0079-6816(93)90013-L. 9

[19] E. J. Verwey, "Theory of the stability of lyophobic colloids," *Journal of Physical and Colloid Chemistry*, vol. 51, no. 3, pp. 631–636, 1947, ISSN: 00223654. DOI: 10.1021/j150453a001. 9

[20] J. Israelachvili, *Intermolecular and Surface Forces*, 3rd. 2011, p. 704, ISBN: 9780123751829. DOI: 10.1016/B978-0-12-375182-9.10025-9. [Online]. Available: http://linkinghub.elsevier.com/retrieve/pii/B9780123751829100259. 9

[21] P. Mundy and B. Madsen, "The development of centrifugal separation technology for tailings treatment Decanter Disc-stack," in *Tailings and Mine Waste*, 2009. 10

[22] C. M. Todaro, "Centrifugation," *Fermentation and Biochemical Engineering Handbook: Principles, Process Design, and Equipment: Third Edition*, pp. 267–281, 2014. DOI: 10.1016/B978-1-4557-2553-3.00013-1. 10

[23] L. Botha and J. B. Soares, "The Influence of Tailings Composition on Flocculation," *Canadian Journal of Chemical Engineering*, vol. 93, no. 9, pp. 1514–1523, 2015, ISSN: 1939019X. DOI: 10.1002/cjce.22241. 12, 14

[24] L. Botha, S. Davey, B. Nguyen, A. K. Swarnakar, E. Rivard, and J. B. Soares, "Flocculation of oil sands tailings by hyperbranched functionalized polyethylenes (HBfPE)," *Minerals Engineering*, vol. 108, pp. 71–82, 2017, ISSN: 08926875. DOI: 10.1016/j.mineng.2017.02.004. [Online]. Available: http://dx.doi.org/10.1016/j.mineng.2017.02.004. 12, 14–16

[25] A. Ariffin, M. A. Razali, and Z. Ahmad, "PolyDADMAC and polyacrylamide as a hybrid flocculation system in the treatment of pulp and paper mills waste water," *Chemical Engineering Journal*, vol. 179, pp. 107–111, 2012, ISSN: 13858947. DOI: 10.1016/j.cej.2011.10.067. [Online]. Available: http://dx.doi.org/10.1016/j.cej.2011.10.067. 12, 14

[26] V. Grumezescu, A. M. Holban, I. Barbu, R. C. Popescu, A. E. Oprea, V. Lazar, A. M. Grumezescu, and M. C. Chifiriuc, *Nanoarchitectonics Used in Antiinfective Therapy*. Elsevier Inc., 2016, pp. 145–166, ISBN: 9780128036686. DOI: 10.1016/B978-0-12-803642-6.00007-1. [Online]. Available: http://dx.doi.org/10.1016/B978-0-12-803642-6.00007-1. 12, 14

[27] S. S. Wong, T. T. Teng, A. L. Ahmad, A. Zuhairi, and G. Najafpour, "Treatment of pulp and paper mill wastewater by polyacrylamide (PAM) in polymer induced flocculation," *Journal of Hazardous Materials*, vol. 135, no. 1-3, pp. 378–388, 2006, ISSN: 03043894. DOI: 10.1016/j.jhazmat.2005.11.076. 12, 14

[28] J. Ma, K. Fu, X. Fu, Q. Guan, L. Ding, J. Shi, G. Zhu, X. Zhang, S. Zhang, and L. Jiang, "Flocculation properties and kinetic investigation of polyacrylamide with different cationic monomer content for high turbid water purification," *Separation and Purification Technology*, vol. 182, pp. 134–143, 2017, ISSN: 18733794. DOI: 10.1016/j.seppur.2017.03.048. [Online]. Available: http://dx.doi.org/10.1016/j.seppur.2017.03.048. 12, 14

[29] G. John, "Polymer adsorption and flocculation in sheared suspensions," *Colloids and Surfaces*, vol. 31, no. 0, pp. 231–253, 1988. DOI: 10.1016/0166-6622(88)80196-3. [Online]. Available: http://www.sciencedirect.com/science/article/pii/0166662288801963. 13

[30] J. Gregory and C. R. O'Melia, "Fundamentals of flocculation," *Critical Reviews in Environmental Control*, vol. 19, no. 3, pp. 185–230, 2009, ISSN: 1040-838X. DOI: 10.1080/10643388909388365. 13

[31] J. Gregory and S. Barany, "Adsorption and flocculation by polymers and polymer mixtures," *Advances in Colloid and Interface Science*, vol. 169, no. 1, pp. 1–12, 2011, ISSN: 00018686. DOI: 10.1016/j.cis.2011.06.004. [Online]. Available: http://dx.doi.org/10.1016/j.cis.2011.06.004. 13

[32] W. Nowicki and G. Nowicka, "Verification of the Schulze-Hardy rule - A colloid chemistry experiment," *Journal of Chemical Education*, vol. 71, no. 7, pp. 624–626, 1994, ISSN: 00219584. DOI: 10.1021/ed071p624. 14

[33] F. O. Garces, K. Sivadasan, P. Somasundaran, and N. J. Turro, "Interpolymer Complexation of Poly(acrylic acid) and Poly(acrylamide): Structural and Dynamic Studies by Solution-and Solid-State NMR," *Macromolecules*, vol. 27, no. 1, pp. 272–278, 1994, ISSN: 15205835. DOI: 10.1021/ma00079a040. 15

[34] H. Li, J. Zhou, R. Chow, A. Adegoroye, and A. S. Najafi, "Enhancing treatment and geotechnical stability of oil sands fine tailings using thermo-sensitive poly(n-isopropyl acrylamide)," *Canadian Journal of Chemical Engineering*, vol. 93, no. 10, pp. 1780–1786, 2015, ISSN: 1939019X. DOI: 10.1002/cjce.22276. 15

[35] L. G. Reis, R. S. Oliveira, T. N. Palhares, L. S. Spinelli, E. F. Lucas, D. R. Vedoy, E. Asare, and J. B. Soares, "Using acrylamide/propylene oxide copolymers to dewater and densify mature fine tailings," *Minerals Engineering*, vol. 95, pp. 29–39, 2016, ISSN: 08926875. DOI: 10.1016/j.mineng.2016.06.005. [Online]. Available: http://dx.doi.org/10.1016/j.mineng.2016.06.005. 15

[36] S. P. Gumfekar and J. B. Soares, "Polymer reaction engineering tools to design multifunctional polymer flocculants," *Chemosphere*, vol. 210, pp. 156–165, 2018, ISSN: 18791298. DOI: 10.1016/j.chemosphere.2018.06.175. 15

[37] M. Kato, M. Kamigaito, M. Sawamoto, and T. Higashimura, "Polymerization of Methyl Methacrylate with the Carbon Tetrachloride/Dichlorotris-(triphenylphosphine)ruthenium(II)/ Methylaluminum Bis(2,6-di-tert-butylphenoxide) Initiating System: Possibility of Living Radical Polymerization," *Macromolecules*, vol. 28, no. 5, pp. 1721–1723, 1995, ISSN: 15205835. DOI: 10.1021/ma00109a056. 17

[38] J. S. Wang and K. Matyjaszewski, "Controlled/"Living" Radical Polymerization. Atom Transfer Radical Polymerization in the Presence of Transition-Metal Complexes," *Journal of the American Chemical Society*, vol. 117, no. 20, pp. 5614–5615, 1995, ISSN: 15205126. DOI: 10.1021/ja00125a035. 17

[39] A. D. Jenkins, R. G. Jones, and G. Moad, "Terminology for reversible-deactivation radical polymerization previously called "controlled" radical or "living" radical polymerization (IUPAC recommendations 2010)," *Pure and Applied Chemistry*, vol. 82, no. 2, pp. 483–491, 2010, ISSN: 00334545. DOI: 10.1351/PAC-REP-08-04-03. 17

[40] *Features of Controlled "Living" Radical Polymerizations - Matyjaszewski Polymer Group - Carnegie Mellon University*. [Online]. Available: https://www.cmu.edu/maty/crp/features.html (visited on 10/07/2019). 20, 32

[41] W. A. Braunecker and K. Matyjaszewski, "Controlled/living radical polymerization: Features, developments, and perspectives," *Progress in Polymer Science (Oxford)*, vol. 32, no. 1, pp. 93–146, 2007, ISSN: 00796700. DOI: 10.1016/j.progpolymsci.2006.11.002. 21

[42] P. V. Mendonça, D. Konkolewicz, S. E. Averick, A. C. Serra, A. V. Popov, T. Guliashvili, K. Matyjaszewski, and J. F. J. Coelho, "Synthesis of cationic poly((3-acrylamidopropyl)trimethylammonium chloride) by SARA ATRP in ecofriendly solvent mixtures," *Polymer Chemistry*, vol. 5, no. 19, pp. 5829–5836, 2014, ISSN: 17599962. DOI: 10.1039/c4py00707g. 21, 22, 31

[43] D. Konkolewicz, Y. Wang, P. Krys, M. Zhong, A. A. Isse, A. Gennaro, and K. Matyjaszewski, "SARA ATRP or SET-LRP. End of controversy?" *Polymer Chemistry*, vol. 5, no. 15, pp. 4396–4417, 2014, ISSN: 17599962. DOI: 10.1039/c4py00149d. 21, 31

[44] *Procedures for Initiation of an ATRP - Matyjaszewski Polymer Group - Carnegie Mellon University*. [Online]. Available: https://www.cmu.edu/maty/atrp-how/procedures-for-initiation-of-ATRP/index.html (visited on 10/22/2019). 21

[45] Y. Y. Durmaz, B. Aydogan, I. Cianga, and Y. Yagci, *Controlled/Living Radical Polymerization: Progress in ATRP*. 2009, vol. 1023, pp. 171–187, ISBN: 0-8412-6995-5. DOI: 10.1021/bk-2009-1023. [Online]. Available: http://www.scopus.com/inward/record.url?eid=2-s2.0-77952854484%7B%5C&%7DpartnerID=tZOtx3y1. 21

[46] Y. Kwak, A. J. D. Magenau, and K. Matyjaszewski, "ARGET ATRP of methyl acrylate with inexpensive ligands and ppm concentrations of catalyst," *Macromolecules*, vol. 44, no. 4, pp. 811–819, 2011, ISSN: 00249297. DOI: 10.1021/ma102665c. 21

[47] P. V. Mendonca, A. S. Oliveira, J. P. Ribeiro, A. Castilho, A. C. Serra, and J. F. Coelho, "Pushing the limits of robust and eco-friendly ATRP processes: Untreated water as the solvent," *Polymer Chemistry*, vol. 10, no. 8, pp. 938–944, 2019, ISSN: 17599962. DOI: 10.1039/c8py01784k. 21, 22

[48] W. Jakubowski, K. Min, and K. Matyjaszewski, "Activators regenerated by electron transfer for atom transfer radical polymerization of styrene," *Macromolecules*, vol. 39, no. 1, pp. 39–45, 2006, ISSN: 00249297. DOI: 10.1021/ma0522716. 21–23

[49] S. H. Ahn, K. S. Cho, J. H. Youk, H. J. Jeon, and J. H. Choi, "Synthesis of high molecular weight 3-arm star PMMA by ARGET ATRP," *Macromolecular Research*, vol. 17, no. 4, pp. 240–244, 2011, ISSN: 1598-5032. DOI: 10.1007/bf03218686. 21

[50] H. C. Lee, M. Antonietti, and B. V. Schmidt, "A Cu(II) metal-organic framework as a recyclable catalyst for ARGET ATRP," *Polymer Chemistry*, vol. 7, no. 47, pp. 7199–7203, 2016, ISSN: 17599962. DOI: 10.1039/c6py01844k. 22

[51] W. Jakubowski and K. Matyjaszewski, "Activators regenerated by electron transfer for atom-transfer radical polymerization of (meth)acrylates and related block copolymers," *Angewandte Chemie - International Edition*, vol. 45, no. 27, pp. 4482–4486, 2006, ISSN: 14337851. DOI: 10.1002/anie.200600272. 22

[52] K. Min, H. Gao, and K. Matyjaszewski, "Use of ascorbic acid as reducing agent for synthesis of well-defined polymers by ARGET ATRP," *Macromolecules*, vol. 40, no. 6, pp. 1789–1791, 2007, ISSN: 00249297. DOI: 10.1021/ma0702041. 22

[53] V. A. Williams and K. Matyjaszewski, "Expanding the ATRP Toolbox: Methacrylate Polymerization with an Elemental Silver Reducing Agent," *Macromolecules*, vol. 48, no. 18, pp. 6457–6464, 2015, ISSN: 15205835. DOI: 10.1021/acs.macromol.5b01696. 22

[54] V. A. Williams, T. G. Ribelli, P. Chmielarz, S. Park, and K. Matyjaszewski, "A silver bullet: Elemental silver as an efficient reducing agent for atom transfer radical polymerization of acrylates," *Journal of the American Chemical Society*, vol. 137, no. 4, pp. 1428–1431, 2015, ISSN: 15205126. DOI: 10.1021/ja512519j. 22

[55] K. Matyjaszewski, W. Jakubowski, K. Min, W. Tang, J. Huang, W. A. Braunecker, and N. V. Tsarevsky, "Diminishing catalyst concentration in atom transfer radical polymerization with reducing agents," *Proceedings of the National Academy of Sciences of the United States of America*, vol. 103, no. 42, pp. 15 309–15 314, 2006, ISSN: 00278424. DOI: 10.1073/pnas.0602675103. 22

[56] K. Matyjaszewski, N. V. Tsarevsky, W. A. Braunecker, H. Dong, J. Huang, W. Jakubowski, Y. Kwak, R. Nicolay, W. Tang, and J. A. Yoon, "Role of Cu 0 in controlled/"living" radical polymerization," *Macromolecules*, vol. 40, no. 22, pp. 7795–7806, 2007, ISSN: 00249297. DOI: 10.1021/ma0717800. 22

[57] K. Matyjaszewski, T. E. Patten, and J. Xia, "Controlled/'living' radical polymerization. Kinetics of the homogeneous atom transfer radical polymerization of styrene," *Journal of the American Chemical Society*, vol. 119, no. 4, pp. 674–680, 1997, ISSN: 00027863. DOI: 10.1021/ja963361g. 23

[58] S. Dadashi-Silab and K. Matyjaszewski, "Temporal Control in Atom Transfer Radical Polymerization Using Zerovalent Metals," *Macromolecules*, vol. 51, no. 11, pp. 4250–4258, 2018, ISSN: 15205835. DOI: 10.1021/acs.macromol.8b00698. 25

[59] H. Ameur, Y. Kamla, and D. Sahel, "Performance of Helical Ribbon and Screw Impellers for Mixing Viscous Fluids in Cylindrical Reactors," *ChemEngineering*, vol. 2, no. 2, p. 26, 2018, ISSN: 2305-7084. DOI: 10.3390/chemengineering2020026. 28

[60] *CST (Capillary Suction Time) test - Degremont®*. [Online]. Available: https://www.suezwaterhandbook.com/water-and-generalities/water-analysis-and-treatability/sludge-examination/CST-Capillary-Suction-Time-test. 30